Mario Fratschko, BSc

Alignment of semiconducting molecular crystals by external electric fields

MASTER'S THESIS

to achieve the university degree of

Diplom-Ingenieur

Master's degree programme: Technical Physics

submitted to

Graz University of Technology

Supervisor

Roland Resel, Ao.Univ.-Prof. Dipl.-Ing. Dr.techn.

Institute of Solid State Physics

Graz, May 2021

AFFIDAVIT

I declare that I have authored this thesis independently, that I have not used other than the declared sources/resources, and that I have explicitly indicated all material which has been quoted either literally or by content from the sources used. The text document uploaded to TUGRAZonline is identical to the present master's thesis.

Date, Signature

Acknowledgements

First of all, I would like to thank my supervisor Roland Resel for enabling me to do this interesting work in his group and also for all the advice he gave me while I was working on this thesis. I am especially grateful for the constant support and the possibility to talk to him personally about my work at any time.
Next, I would like to thank all the members of the Resel and Coclite groups, as they gave me a lot of important information for my experiments and for the theoretical elaboration of my work. I am especially grateful to Martin Kaltenegger, Wolfgang Bodlos, Sebastian Hofer, Valentin Holzer, Ann-Maria James, Manuel Kainz and Lukas Legenstein who were always available if questions appeared.
For the experimental assistance and the joint repair of the vacuum chamber I would like to thank Harald Kerschbaumer, who always took time for me and explained every component of the vacuum chamber to me in great detail.
Finally, I would like to thank my parents and siblings, as well as my friends, for their constant support during all the years I have been studying. Without you I would not have come so far and I am very glad that I have you.

Abstract

The ability to control crystallization for easier and cheaper fabrication is technologically important in many fields e.g. in pharmacy or food industry. Interaction with an electric field would be one method, since one can vary the electric field strength as well as the direction of the electric field. In this work the interaction of semiconducting organic molecules with an electric field, generated with direct voltage, is investigated, and furthermore, how these molecules crystallize in this environment is also studied. The experiments are performed by crystals grown at a substrate. Thin films are prepared by physical vapour deposition and subsequently treated by solvent vapour annealing (SVA). Three different molecules (2-decyl-7-phenyl-[1] benzothieno[3,2-b][1] benzothiophene, 2-decyl-7-phenyl-[1]benzothieno[3,2-b][1] benzothiophene S,S,S',S'-tetraoxide, quinquethiophene) are used in combination with an interdigitated electrode structure. The distance between the electrodes is in the range of 10 μm for the gold substrates and 50 μm to up to 200 μm for the tin doped In_2O_3 substrates. For the SVA experiment, toluene and chloroform are used. However, chloroform is mainly used, since more interesting results are obtained with this solvent. The thin films are investigated by atomic force microscopy, optical microscopy, X-ray reflectivity and with grazing incidence X-ray diffraction. We found that an electric field reduces the nucleation density upon crystallization, which was predicted from theory and already confirmed experimentally. For the molecule 2-decyl-7-phenyl-[1]benzothieno[3,2-b][1] benzothiophene S,S,S',S'-tetraoxide also a larger crystal size is confirmed in an electric field environment. Addditionaly for this molecule, a rod-like growth of the crystals along the electric field is observed. Furthermore, we found that the crystals are formed at the edges of the electrodes with strong preferred orientation of the organic crystals. However, this second observation cannot be unambiguously referred to the impact of the electric field, since nucleation at step edges is a competing crystal growth effect.

Kurzfassung

Die Fähigkeit, die Kristallisation für eine einfachere und kostengünstigere Herstellung zu steuern, ist in vielen Bereichen technologisch wichtig, z. B. in der Pharmazie oder der Lebensmittelindustrie. Die Wechselwirkung mit einem elektrischen Feld wäre eine Methode, da man sowohl die elektrische Feldstärke als auch die Richtung des elektrischen Feldes variieren kann. In dieser Arbeit wird die Wechselwirkung von organischen Molekülen mit einem elektrischen Feld, das mit Gleichspannung erzeugt wird, untersucht und darüber hinaus, wie diese Moleküle in dieser Umgebung kristallisieren. Die Experimente werden an Kristallen durchgeführt, die auf einem Substrat gebildet werden. Die dünnen Schichten werden durch physikalische Gasphasenabscheidung hergestellt und anschließend durch Lösungsmitteldampfglühen behandelt. Drei verschiedene Moleküle (2-decyl-7-phenyl-[1] benzothieno[3,2-b][1] benzothiophene,2-decyl-7-phenyl-[1]benzothieno [3,2-b][1] benzothiophene S,S,S',S'-tetraoxide und Quinquethiophene) werden in Kombination mit einer interdigitalen Elektrodenstruktur verwendet. Der Abstand zwischen den Elektroden ist im Bereich von 10 μm für die Gold-Substrate und zwischen 50 μm und 200 μm für die ITO-Substrate. Beim Lösungsmitteldampfglühen-Experiment werden Toluol und Chloroform als Lösungsmittel verwendet. Im weiteren Verlauf wird jedoch hauptsächlich Chloroform verwendet, da mit diesem Lösungsmittel interessantere Ergebnisse erzielt werden. Diese Experimente werten wir mit Rasterkraftmikroskopie, mit einem Lichtmikroskop und mittels Röntgenbeugung aus. Wir fanden heraus, dass ein elektrisches Feld die Keimbildungsdichte reduziert, was aus der Theorie vorhergesagt und bereits experimentell bestätigt wurde. Für 2-decyl-7-phenyl-[1]benzothieno[3,2-b][1] benzothiophene S,S,S',S'-tetraoxide ist auch die Kristallgröße bei der Kristallisation größer. Zusätzlich wird bei diesem Molekül mit dem Lichtmikroskop ein stäbchenförmiges Wachstum der Kristalle entlang des elektrischen Feldes beobachtet. Weiters haben wir festgestellt, dass die Kristalle an den Kanten der Elektroden gebildet werden, wobei die organischen Kristalle stark bevorzugt orientiert sind. Diese zweite Beobachtung kann jedoch nicht eindeutig auf den Einfluss des elektrischen Feldes auf Keimbildung an Stufenkanten bezogen werden.

Contents

1 Introduction

An electric field, caused by electric charges, exerts a force on electrically charged particles, either attracting or repelling them, depending on the sign of the charge.[Roc16] Michael Farady (1791-1867) developed a concept to visualize the electric field. The field is represented by a set of lines pointing in the direction of the electric field. The field strength is proportional to the density of the field lines, i.e. if the density of the lines is small (large distance between the lines) the field strength is small.[Far55] When there is a positive charged particle in the electric field, it is moved in the direction of the field lines due to the force acting on it. The force felt by such a charge q_1, in a stationary electric field of another charged particle q_0, is described by the combination of Gauss's law and Faraday's law of induction and is equivalent to the Coulomb's law: [PM13]

$$\vec{F} = \frac{1}{4\pi\epsilon_0} \frac{q_1 q_0}{(x_1 - x_2)^2} \vec{r_{1,0}} \tag{1.1}$$

where ϵ_0 is the electrostatic constant and $r_{1,0}$ is the unit vector from the point x_1 to x_2. The electric field in contrast at a point x_0 is the Coulomb force divided by the charge q_0:

$$\vec{E}(x_0) = \frac{\vec{F}}{q_0} = \frac{1}{4\pi\epsilon_0} \frac{q_1}{(x_1 - x_2)^2} \vec{r}_{1,0} \tag{1.2}$$

In order to describe the behavior of molecules in an electric field, the dipole moment $\vec{m}$ is used, which is a measure of the separation of positive and negative charges q in a system and is described by the following formula, when using the simple modle for a molecule:

$$\vec{m} = q * \vec{d} \tag{1.3}$$

where d is the distance between the charges. For example, if a polar molecule (one end is positively charged and the other end is negatively charged) is in such an electric field caused by two charged plates, the positive end of the molecule will be directed toward the negatively charged plate and the negative end of the molecule will be directed toward the positively charged plate. Consequently, the molecule is oriented along the electric field [Pol] Non-polar molecules, which do not have a dipole moment, also orient themselves in an electric field. The electric field causes a charge shift in the molecule, which is also called displacement polarization α, and thus induces a dipole moment $\vec{m}$ which is described by the following formula:[Hei16]

$$\vec{m} = \alpha * \vec{E} \tag{1.4}$$

In order to orient a single molecule in the direction of the electric field, its potential energy eq. 1.5 [SJ09] must be greater than its kinetic energy eq. 1.6. [Kin]

$$E_{pot} = -\vec{m} * \vec{E} \tag{1.5}$$

$$E_{kin} = \frac{1}{2} k_B T \tag{1.6}$$

where the potential energy E_{pot} depends on the dipole moment $\vec{m}$ and the kinetic energy E_{kin} is from the equipatitions theorem and is proportional to the Boltzmann constant k_B and the temperatur T in the system. Knowing the relative permittivity of a material, one can use the Clausius-Mossotti equation [Rys02] to calculate the displacement polarization α. Thus, for SiO_2 the displacement polarisation would be $\alpha = \frac{1{,}31}{N} \frac{Cm^2}{V}$ where N is equal to the number of particles per cubic meter. Thus, SiO_2, at an electric field of $E = 10^7 \frac{V}{m}$, has a dipole moment of $\vec{m} = \frac{1.31*10^7}{N} D$.

The electric field not only affects the displacement of charges or the orientation of individual molecules, it also influences the crystallization process by affecting nucleation. [Kas00] Crystallization occurs when the chemical potential of the solid phase is lower than that of the liquid or gaseous phase. The chemical potential difference, also called supersaturation factor, is the thermodynamic driving force for crystallization described with following equation:[MS77]

$$\Delta\mu = \mu_g - \mu_s \tag{1.7}$$

where μ_g is the chemical potential of the gas phase and μ_s is the chemical potential of the solid phase. If this crystallization takes place in an electric field, the supersaturation factor $\Delta\mu$ changes to a factor which depends on the electric field:

$$\Delta\mu_E = \Delta\mu + c_e E^2 \tag{1.8}$$

with

$$c_e = \frac{\epsilon_0 \epsilon_g}{2}(1 - \frac{\epsilon_g}{\epsilon_s}\nu_0) \tag{1.9}$$

where E is the electric field, ϵ_0 is the vacuum permittivity, ϵ_g and ϵ_s are the relative permittivities of the gas and solid phase and ν_0 is the molecular volume. If the function c_e is positive, i.e. the relative permittivity of the solid phase is greater than that of the gas phase, than the nucleation is enhanced and if c_e is negativ than nucleation is impeded by the electric field. The exact derivation of the calculation is described in the book by Dimo Kashchiev.[Kas00]
In 1999, Taleb et al.[Tal+99] found that the electric field has an effect on the size

and number of crystals. Fewer but larger crystals are obtained than in crystallization without electric field, thus an improvement in the quality of the crystals is observed. Furthermore, according to L. Alexander and N. Radacsi,[AR19] the electric field reduces the time for nucleation and, in addition, control of the position of nucleation, control of the orientation of the crystals and control of polymorphism should be possible.

2 Fundamentals

2.1 Physical vapor deposition

Physical vapor deposition is a deposition technique using a source gas produced by physical processes like evaporation of a meterial in a vacuum. In the evaporation process, a target material is heated until it goes from a condensed phase to a vapor phase and on the substrate back to a condensed phase. [Pvd] In the following chapter it is described in more detail.

2.1.1 Evaporation

Evaporation can be distinguished between different applications and ranges from simple resistance heaters in a high vacuum to molecular beam epitaxy in ultra high vacuum, whereas the former is of more importance for our studies. In the resistance heater methode one produces the vapor flux in substrate direction simply by heating a target material with a hot filament source. In order to heat the source with an resistance heater an electric current is passed through it. There are different types of sources, which are described in a latter section. The required pressure for this high vacuum system is between 10^{-5} $mbar$ to 10^{-8} $mbar$. This vacuum range is required to have a large mean free path λ, which is the distance between two collisions of the evaporated particles. This means that in this vacuum range there are no collisions between the molecules at the distance from the source to the substrate[Pvd]. So without any scattering, the evaporant condensates on the substrate forming a thin film. The formula for the mean free path is given by:[KV65]

$$\lambda = \frac{RT}{\sqrt{2}\pi d^2 N_A p} \tag{2.1}$$

Where R is the gas constant, T is the temperature, d is the diameter of the molecules, N_A is the Avogadro number and p is the pressure in the chamber.
A further important quantity in physical vapor deposition is the impingment rate z. This indicates how many collisions there are with the surrounding area (vacuum chamber or substrate). The unit for this rate is collisions per area per second and it is proportional to the pressure p:[Mah00]

$$z = \frac{p}{2\pi k_B T} \tag{2.2}$$

where m is the mass of the particles, k_B is the Boltzmann constant and T is the tem-

perature inside the vacuum chamber. With this two quantities, the mean free path and impingment rate, one can choose the required vacuum for the physical vapor deposition chamber.
The experimental setup for physical vapor deposition as in fig. 2.1 schematicaly shown basically consists of a vacuum chamber with an associated pumping system, an evaporation cell, which is mostly placed in the base of the chamber, and a substrate holder. For more precise evaporation, a quartz microbalance is used to control the gas flux. The quartz microbalance uses a frequency-dependent quartz crystal to indirectly measure the vapor-deposited layer thickness. When particles strike the crystal, its mass is increased and thus its resonant frequency is changed. The frequency change is proportional to the layer thickness of the vaporized substance and can be calculated using the Sauerbrey equation:[Sau59]

$$\frac{\Delta f}{f} = -\frac{\Delta d}{d} = -\frac{\Delta m}{\rho A d} \tag{2.3}$$

where f is the Eigenfrequenz (Hz) of the quartz crystal, Δd (cm) is the thickness of the evaporated film, d (cm) is the thickness of the quartz crystal, Δm is the mass of the covering film, ρ ($\rho = 2.648\ \frac{g}{cm^3}$) is the density of the quatz crystal and A (cm^2) is the area of the crystal. To further optimize the process, a so-called shutter can be used to shield the substrate during the gas flow adjustment. [Pvd]

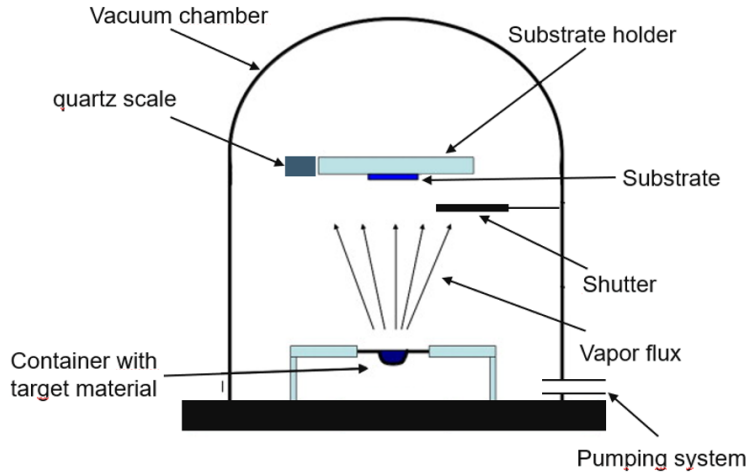

Figure 2.1: Simplified schematic illustration of a physical vapor deposition setup. [MPL13]

2.1.2 Experimental setup

In our experiments we use the same setup as in fig. 2.1 with the exception of a shutter. In fig. 2.2 the experimental setup is depicted with the substrate holder (1), which is attached to an 8 cm spacer (2) to the upper chamber closure (3). The reason for the

spacer is that the molecules do not reach the top and condense at a lower levels because the vacuum chamber may have a leak. There are two wires (4) soldered to the substrate holder. These are needed to apply an electrical voltage to the substrate in order to generate an electrical field on the substrate. The used substrates are described in a latter section. To the right of the spacer, there is the quartz crystal microbalance (5), which is attached to a copper tube (6). Since no copper tube was found to attach the quartz scale to the same height as the substrate holder, the quartz scale is 3 cm above the substrate holder. The pressure in this setup is achieved with a pumpsystem consisting of a rotary vane pump (10^{-3} $mbar$) and a turbomolecular pump (10^{-10} $mbar$). The rotary vane pump is used to prevent damage to the turbomolecular pump because its operating range is between 10^{-1} $mbar$ and 10^{-10} $mbar$.

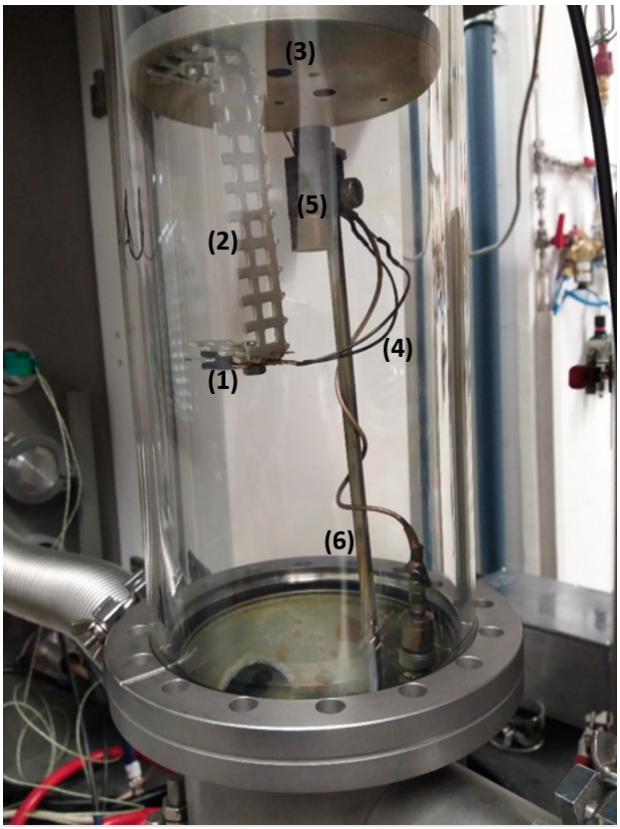

Figure 2.2: Vacuum chamber with (1) substrate holder, (2) spacer, (3) top of the vacuum chamber, (4) wires for voltage conection, (5) quartz scale and a (6) copper tube.

The sample holder is depicted in fig. 2.3 in more detail and it consists of a plastic housing with copper connections. The substrate is inserted into this housing in order to mechanically connect its electrodes with the copper wires. The wires for the power supply are soldered to the copper wires. This substrate holder was chosen because it is very easy to supply the electrodes of the substrate with voltage and, in addition, it is

a fast and safe setup in the vacuum chamber. The substrate holder is screwed to the spacer which is in turn screwed to the top of the vacuum chamber to prevent as much gas entrapment as possible.

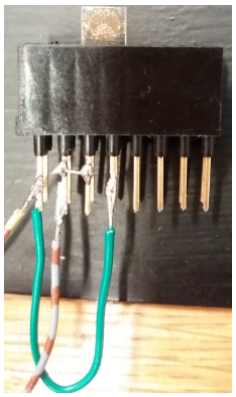

Figure 2.3: sample holder with gold substrate in it and breeded wires to conect with power supply

For the material source two different types were used. Both sources have small capacities resulting in refilling them after every evaporation process. The first one in fig. 2.4 is a kind of a Knudsen cell made of a cut quartz glass, with a small opening hole, wrapped with a tungsten wire. The ends of the wire are connected to a power line which heats the wire by means of an electric current. Since the wire is very thin, only small currents of the order of 3.4 A are needed to reach the vaporization temperature of organic semiconductors. The temperature of the wire is transferred to the quartz vessel, but this process takes a long time because the heat conduction coefficient of the glass is low. The advantage of this cell is that it has a directed molecular beam towards the substrate and therefore less material is wasted. The disadvantage is that it takes a long time for the material to evaporate, making the molecular flow difficult to control.

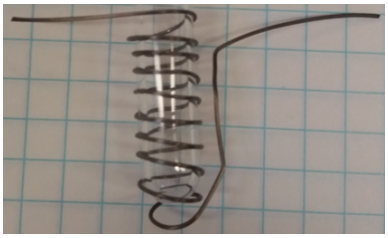

Figure 2.4: Knudsen cell from quartz glass wrapped with a tungsten wire

The second container as can be seen in fig. 2.5 is a tungsten evaporation boat, which is also connected to a power source. To heat this boat, a higher current of at least 60 A is required to reach the same temperature as with the tungsten wire. Since this boat heats up faster, the gas flow can be controlled better. Unlike the Knudsen cell, this boat

does not have a directional beam and therefore requires more material to achieve the same film thickness on the substrate.

Figure 2.5: Target tungsten source to heat material.[Tun].

2.2 Solvent vapor annealing

To produce organic semiconductor films there are different possibilities like deposition methods (PVD) or solvent processing like drop casting or spin coating. With these methods defects can occur such as non-uniform thicknesses, dislocations or molecular disordering. To improve the quality of the film by reducing the defects, post-treatment methods are used.[DL+10] On the one hand, thermal annealing is used, in which the material is exposed to high temperature for a certain time. This causes the atoms or molecules to migrate,which results in decreaing of the dislocations of the thin film. After a certain time, the material is slowly cooled.[The] When using thermal annealing on organic semiconductors, degradation can occur due to the high temperatures involved. On the other hand, in order to avoid such degradation, solvent vapor annealing is used. In solvent vapor annealing, the coated substrates are positioned on a sample holder at room temperature in a solvent vapor saturated environment, as schematically shown in fig. 2.6. It is important that the chamber is airtight sealed. After a period of time, the surface of the thin film is partially re-solubilized. This allows the molecules a long range migration and this leads to a restructured thin film of a higher degree of order, reduced defect density and improved lateral order. The reorganization of the molecules depends strongly on the solvent used, as this has an influence on the various interactions between the molecule, solvent and substrate. [DL+10]

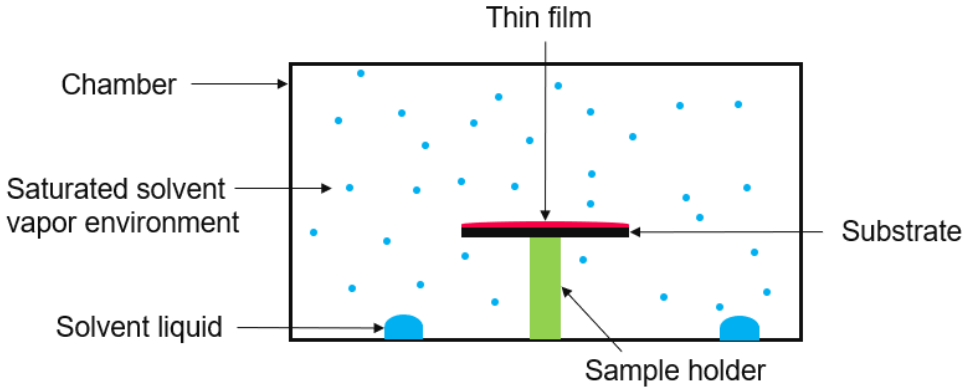

Figure 2.6: Schematically illustrated solvent vapor annealing setup. The substrate with the thin film is positioned in a closed chamber on a substrate holder. This chamber is filled with solvent until the environment is saturated with it.

Using an electric field generated with closely spaced electrodes ($d \sim 50\ \mu m$) in the solvent vapor annealing process can affect the crystal orientation. Due to the solvent, molecules move more easily and so for example organic semiconductor single crystals can grow in the direction of the electric field. As a consequence, the mobility of the electrons of these crystals is higher than without electric field.[KOS16]

2.2.1 Experimental setup

For these experiments, the substrates previously processed with physical vapor deposition are used. Two conductive wires are then soldered to the electrodes of the substrate to create an electric field on it. Two Petri dishes of the same size, cleaned with acetone and isopropanol, are used for the chamber. The sample is placed in the center of the Petri dish and the wires are bent, as shown on the left side in fig. 2.7, until the substrate is horizontal to the bottom plane of the dish. Afterwards, the second dish is put on top of the first and the half of both dishes are wraped with a parafilm tape. Once the Petri dishes are connected, two croco plugs from a voltage source are applied to the wires. Then the chamber is filled with solvent using a syringe and the second half of the chamber is then closed airtight with parafilm tape. Once everything is sealed, the voltage source is switched on. No substrate holder is needed for this setup, as the wires are pinched between the two Petri dishes and thus the substrate levitates in the air. Once the experiment is complete, the voltage source is turned off and the chamber is carefully opened.

Figure 2.7: Solvent vapor annealing setup from the side (left) and from the top (right). The chamber consists of two Petri dishes connected with a para tape. The wires are connected to a voltage source as can be seen in the right picture.

2.3 Atomic force microscopy

An atomic force microscope (AFM) is a microscope for three-dimensional imaging of a sample with very high resolution and very high accuracy at an atomic level. Unlike an optical or electron microscope, which require a focus of light or electrons, an AFM interacts mechanically with the surface of a sample by means of a sharp tip, while the tip oscillates at very high frequencies. With this principle, almost all materials (from hard ceramics to soft DNA) can be measured. The AFM consists basically as can be seen in fig. 2.8 of a laser, a cantilever with a sharp tip, a position sensitive photodetector and a piezo scanner. To acquire an image, the sample is moved with the piezo scanner and a laser hits the back side of the cantilever. The deflection of the cantilever due to the forces between the tip and the sample is recorded by the photodiode and a topographic image of the sample is obtained. Depending on the operation mode, the tip has different distances (0 - 10 nm) to the substrate, with the minimum being at the contact mode and increasing with the tapping mode to the non-contact mode. The advantage of the oscillating modes to the contact mode is that the tip-sample force is reduced while the sensitivity to topography remains the same. The measuring range of an AFM is between 5 nm and 100 μm. The upper limit is determined by the fact that an AFM scans mechanically and this would take too much time above 100 μm. Since almost no sample preparation is needed and measurements can be made in any environment (vacuum, ambient atmosphere), an AFM is easy to use.[EW10]

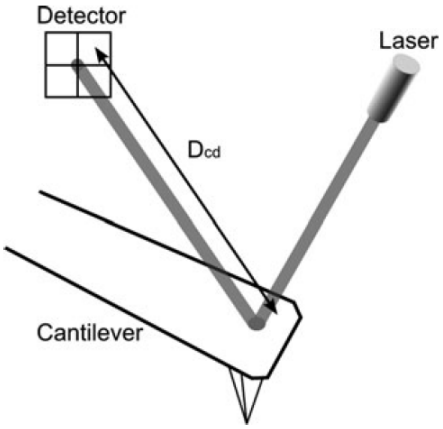

Figure 2.8: Schematically illustrated atomic force measurement with a laser, a cantilever with a sharp tip and a photodetector. [EW10]

2.3.1 Experimental setup

In order to be able to measure with the atomic force microscope (Nanosurf easy scan) as can be seen in fig. 2.9, a computer and an electronic control unit are also required. The latter is connected to both the microscope and the computer. The control unit is used to move the scanner and all other motorized components of the AFM. In addition, the electronic unit digitizes the signals from the measurement to display them on the computer. The microscope stage in turn consists of a sample holder, a piezoelectric scanner to move the sample, and a measuring head to which the measuring tip is attached. To move the measuring tip close to the specimen, one turns the screws attached to the measuring head. It should be noted that the measuring head must always be parallel to the microscope stage, otherwise inaccurate images will be obtained. An optical microscope is often attached to the measuring head to monitor the movement of the tip to the specimen. Furthermore, a vibration absorber is used to minimize ambient vibrations and improve resolution. On the computer, with the software program Nanosurf easy scan the parameters for the measurement are set, which are transferred to the control unit. First of all the used measuring head is set in the program (if there are several possibilities). Second, the set point is adjusted, which is a measure for the tip sample force. With a high set point, the force between the tip and the specimen is greater, which means that the deflection of the laser beam is greater. With a small set point, the reverse is true. Subsequently, in order to improve the quality of the image, the scanning speed and the number of measuring points per line are adjusted. In order to obtain a correct signal, the parameters P-Gain (proportional gain, should be higher than 1000), the I-Gain (integrated gain, should not exceed one tenth of the P-Gain) and the free vibrational amplitude (higher than 50 mA) must be varied and adapted to the sample to be measured, since there is no exact specification of these parameters. The program Gwyddion [Gwy] is used to analyze the measurements.

Figure 2.9: Setup for the AFM measurement with the (1) computer, the (2) electronic contol unit, the (3) AFM stage, the (4) vibration absorber and the (5) measuring head.

2.4 Optical microscopy

Light microscopes are microscopes that can greatly magnify small structures using light. In this process, the sample is illuminated with white or monochromatic light. Magnification is accomplished with a lens system and the associated laws of optics. First, a converging lens (objective) creates a real image between the objective and the eyepiece (fig. 2.10). Then, the stage is adjusted until the magnified image of the converging lens is moved exactly into the focal plane of the eyepiece. As a result, the eyepiece does not produce a real image but "parallels" the rays coming from the objective image, causing our eye to perceive the image at infinity. This makes the image appear so pleasing to our eye.[KTW19]

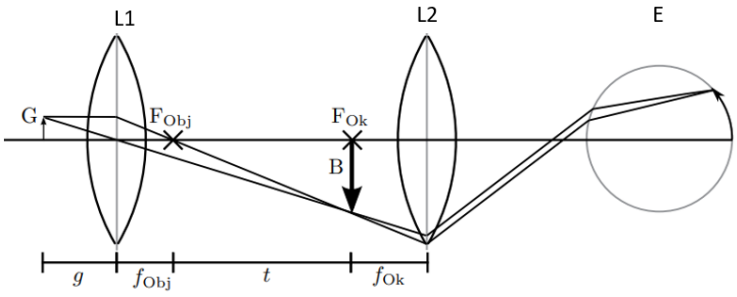

Figure 2.10: Optical imaging with the aid of the lens system with the objective L1, the eyepiece L2 and the eye E.[KTW19]

The total magnification of the object is calculated using the two individual magnifications of the lenses and then multiplying them together. The formula for the magnification

is as follows:[KTW19]

$$V = \frac{t * s_0}{f_{Obj} * f_Ok} \tag{2.4}$$

Where V is the magnification of the microscope, t is the optical tube length, s_0 is the reference distance of 25 cm, f_{Obj} is the focal length for the object and f_{Ok} is the focal length for the eyepiece.

2.4.1 Experimental setup

In addition to the optical microscope, the entire setup consists of a camera and a computer with the necessary software for capturing images. The basis is the Olympus BX51 microscope which can be seen in fig. 2.11 and it can not only capture reflected light but also transmitted light. In transmitted mode, the substrate lying on the stage is illuminated with light from below and a so-called negative image is obtained. The stage can be moved in all three spatial directions with a coarse drive and a fine drive, in order to be able to measure the sample at the correct position. Furthermore, the microscope has a turret with different magnifications in it ranging from 5x to 100x magnification. In addition, it also has various polarization filters and apertures to view certain areas more closely. To determine the intensity of the incident light and to change the brightness of the image, a control is installed on the right side of the microscope.

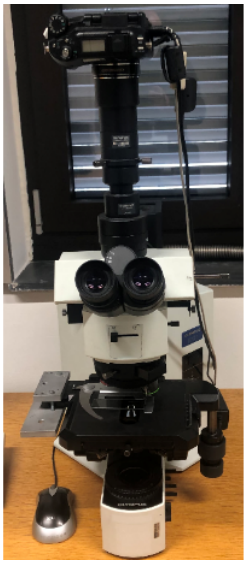

Figure 2.11: Optical microscope Olympus BX51 with camera on top

With the camera, which is connected to the lens system, photos are taken. The taken photos are saved on the computer with the Olympus Stream software. Apart from saving the images, the program can be used to view the probe as through the eyepiece and edit

the captured images.

2.5 Scattering of X-rays

In order to measure the distances of atoms in a solid, which are in the range of one Angström, beams with a smaller wavelength than the atomic distance must be used. The rays used for this are called X-rays and are electromagnetic waves between a wavelength range of 10 nm (soft X-rays) to 10 pm (hard X-rays). This radiation is generated either by acceleration (bremsstrahlung, synchotron radiation) or by high-energy transitions in the electron shells of atoms. Whereby the latter is the characteristic X-ray radiation and has a line spectrum. When matter is irradiated with X-rays, these rays are scattered by the electrons of each atom and subsequently interfere with each other. [SC93] This is the basic principle in X-ray diffraction on crystals and it is called Bragg's law which is described by the following equation: [BB13]

$$n\lambda = 2d_{hkl}sin(\theta) \tag{2.5}$$

where n is an integer number, λ is the wave length of the used x-rays, d_{hkl} is the inter-planar distance, θ is the scattering angle and h, k and l are the Miller indices describing equidistant planes in the crystal. The Bragg equation describes when constructive interference of waves occurs when scattering from a three-dimensional lattice. To understand it better, the geometric principle is shown in fig. 2.12. An incoming beam is reflected at the electrons of an atom in a crystal lattice, where the distance of the individual lattice planes to each other is d_{hkl}. A second beam hitting an atom on the second level has to travel an additional distance of $2 * d_{hkl}sin\theta$. To obtain constructive interference and thus to be able to measure the reflected beam with a detector, the additional distance from the second beam must be an integer multiple of the wavelength of this radiation.

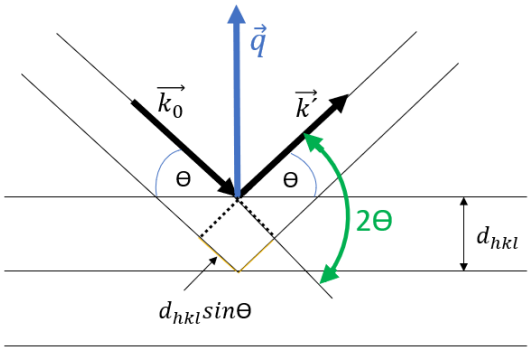

Figure 2.12: Schematic illustration of the geometric principle of Bragg´s law

The same principle, but in reciprocal space, is seen in the Laue condition. This states that diffraction occurs when a vector $\vec{q}$ is equal in magnitude to the reciprocal lattice

vector $\vec{G}$. The vector $\vec{q}$, also called scattering vector, is defined as the difference between incoming and outgoing wave vector:[FKL13]

$$\vec{q} = \vec{k'} - \vec{k_0} \tag{2.6}$$

For elastic scattering ($|\vec{k_0}| = |\vec{k'}| = \frac{2\pi}{\lambda}$) , an expression for the scattering vector is obtained which is independent of the wavelength used:

$$|\vec{q}| = q = \frac{4\pi}{\lambda} sin(\frac{2\theta}{2}) \tag{2.7}$$

2.5.1 Specular X-ray reflectivity (XRR)

X-ray reflectivity is a non destructive surface sensitive method for the investigation of thin films. Here the angles of the incoming and outgoing beam are the same and thus the scattering vector is perpendicular to the substrate surface as can be seen in fig. 2.12 and out of plane information is obtained. [Mit09] In this method the incoming beam has a small anlge between 0° and 6°. When the X-rays hit a sample, the reflection can be described by the index of refraction n:[SG13]

$$n = 1 - \delta + i\beta \tag{2.8}$$

with a dispersion term

$$\delta = \frac{\lambda^2}{2\pi} r_e \rho_e \tag{2.9}$$

and an absorption term

$$\beta = \frac{\lambda}{2\pi} \mu_x \tag{2.10}$$

where λ is the used wavelength of the x-rays, $r_e = 2.818 * 10^{-15}\ m$ is the electron radius, ρ_e is the electron density of the examined material and μ_x is the absorption length. If δ is larger than 0 than the refractive index is smaller than 1 and so we have total external reflection which occurs for incident angles α_i smaller than the critical angle which is:

$$\alpha_c = \sqrt{2\delta} \tag{2.11}$$

Due to the fact that δ is mostly in the range between 10^{-5} and 10^{-6} leads to a critical angle α_c between 0.1° and 0.5°.[SG13] Is the angle of irradiation greater than the critical

angle, than the x-rays will transmit into the sample until they reach the substrate. If the electron density of the film is constant and the angle of incidence is varied, a periodic signal is seen as in fig. 2.13, which shows the XRR curve of Ph-BTBT-Ox_2 on a glass substrate with ITO electrodes on it.

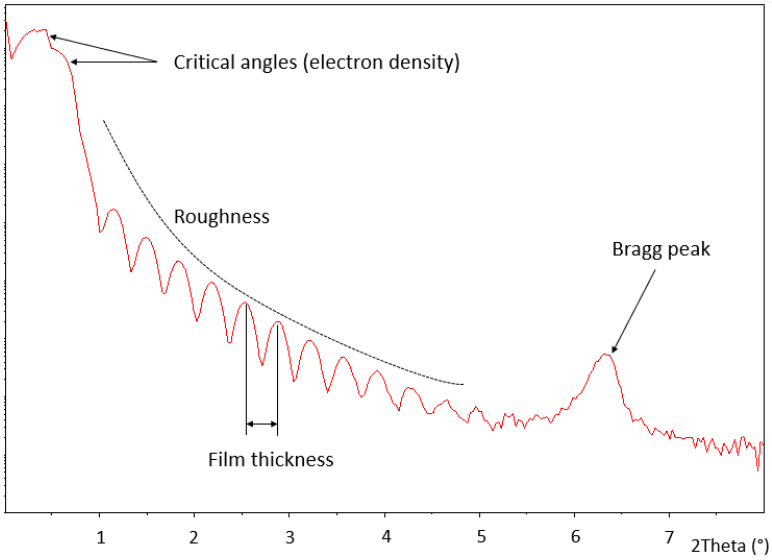

Figure 2.13: XRR diffraction pattern of Ph-BTBT-Ox_2 on an ITO/glass substrate with the gained information from it

With this measurement the electron density, the thin film thickness, the surface roughness and the crystal phase orientation can be determined.[Ina08] The electron density is calculated from the eq. 2.11 by excluding the position from the critical angle. The film thickness is obtained from the width of the periodic peaks also called Kiessig fringes.[Kie31] The surface roughness is related to the slope of the curve and the crystal phase orientation is obtained from the Bragg peak.

2.5.2 X-ray reflectivity experimental setup

The experiments are done with a PANalytical Empyrean X-ray diffractometer as can be seen in fig. 2.14. The first component of the diffractometer is a X-ray tube, which emits Cu-Kα radiation with a wave length of $\lambda = 1.54056\ \mathring{A}$ at 40 kV voltage and 40 mA current. The second component is a parallel beam mirror, which parallelize the incident X-rays. Next is a beam attenuator, which limits the beam intensity on the detector with a 0.125 mm Ni-plate, which attenuation coefficient is precisly known. It switches electricaly on when the intensity surpasses 900000 counts. Furthermore, in this setup, we have the sample table, where we put our samples on. It can be rotated and tilted with a software and this also also during the experiments. To recive a signal a PANalytical PIXcel Solid State Detector is use. With this detector the number of measuring channels can be altered so that it can be used as a scanning point- or also as a line detector. Next

in this setup is a goniometer, with which the detector as well as the incoming beam can be moved to different angles with an accuracy of 0.0001 °. In order to reduce the beam divergence a divergence slit (1/8 or 1/32) can be used and for limiting the beam width a beam mask (4 mm, 10 mm or 20 mm) is used. The last component is an anti-scatter slit (0.1 mm or 7.5 mm), which reduces the background signal from scattered X-rays.

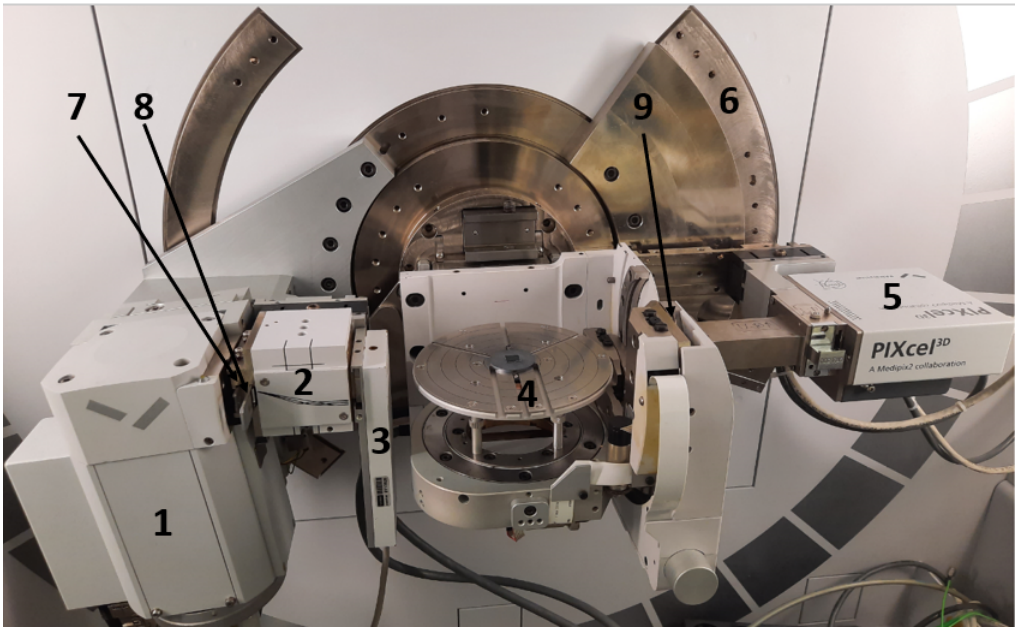

Figure 2.14: Experimental setup for the XRR measurements with (1) the X-ray source, (2) the parallel beam mirror, (3) the beam attenuator, (4) the sample table with a sample, (5) the X-ray detector, (6) the Goniometer, (7) the divergence slit, (8) the beam mask and (9) the anti-scatter slit

2.5.3 Grazing Incidence X-Ray Diffraction (GIXD)

GIXD is a surface sensitive method with a small angle of the incoming beam, which is in the range of the critical angle. Below the critical angle, there is total reflection and instead of X-rays, the diffraction of an evanescent wave, generated on the surface, is detected. These evanescent waves are exponentially attenuated from the surface, limiting the penetration depth. In contrast to XRR, with this method also in-plane oriented films can be investigated. As can be seen schematically in fig. 2.15, a fixed incoming beam described with the wave vector $\vec{k_0}$ hits the sample at an angle α_i. The outgoing beam described by the wave vector $\vec{k}$ is neither in the same plane nor does it have the same angle as $\vec{k_0}$. The corresponding scattering vector $\vec{q}$ can be calculated with eq. 2.6. The result of such an experiment is the measured intensity as a function of the scattering vector and is represented in a reciprocal space map. If a sample, which has defined in

and out of plane aligned crystals, is measured at a certain position, not all diffraction information is obtained. To avoid this and to get more data the sample is rotated in the x-y plane (rotating GIXD).[WH95]

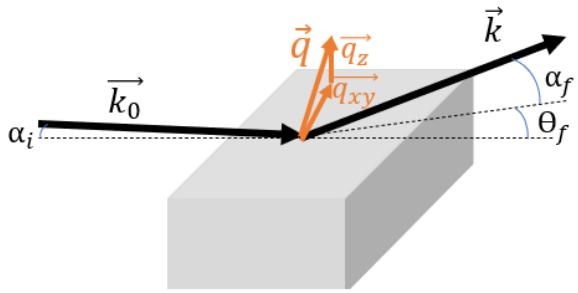

Figure 2.15: Shematical illustristration of the basic principle of GIXD [Wan+06]

2.5.4 GIXD experimental setup

The experiments were performed with the Elettra synchotron at the XRD1 beamline in Trieste. The used detector there is a Dectris Pilatus 2M detector, which map a two dimensional section of k-space. More details about the further construction can be found on the website of Elettra.[Ele]

2.6 Interdigitated substrate

Interdigitated substrates are made of two individually addressable electrodes, with microelectrode array strips, which are placed close to each other. As a result the distance between the two electrodes can be reduced to a small value (e.g. 5 μm). These interdigitated electrodes are mostly used for impedance, capacitance and conductivity measurements. In our experiment, a voltage is applied to one electrode and the other electrode is connected to ground, creating a voltage difference between the two electrodes and forming an electric field between them. Two different substrates are used, the first with gold electrodes and the second with doped indium tin oxide (ITO) electrodes.

2.6.1 Gold

The gold electrode substrate is from Micrux technologies and is depicteted in fig. 2.16. It is a glass substrate with a 10 x 6 x 0.75 mm dimension. It has 90 electrode pairs with a height of 150 nm. The electrode thickness and the distance between the electrodes is 10 μm. Around the electrodes there is layer which is a SU-8 resin protective layer. In fig. 2.17 it is depicted in more detail. The small yellow stripes are the 10 μm thick electrodes and the black ring is the end of the SU-8 protective layer that does not protect the fingers but the outer electrodes and it ends bevor the contacts.[Inta]

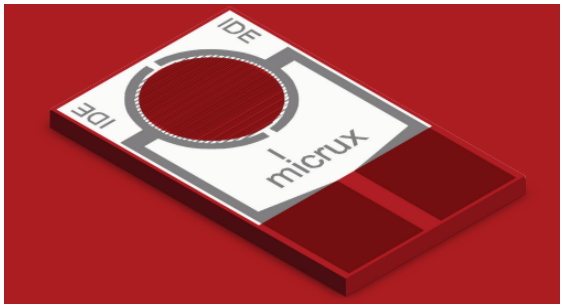

Figure 2.16: Picture of the glass substrate with gold electrodes on it, where the white layer is the SU-8 protective layer.[Inta]

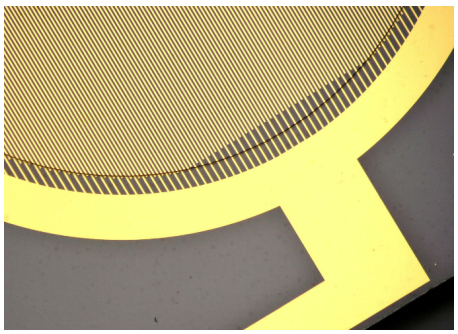

Figure 2.17: Picture of the right side of the gold substrate taken with the optical microscope at fivefold magnification, where the black ring is the end of the SU-8 protective layer.

The electric field E between the electrodes is calculated with following equation:

$$E = \frac{U}{d} \tag{2.12}$$

where U is the voltage difference between the electrodes and d is the distance between the electrodes.[Poh13] The maximum voltage that can be applied during PVD experiments is 180 V. If the voltage is higher, due to short circuits, sparks will be generated and the gold will evaporate. Therefore the maximum electric field which can be generated is $E = 1.8 * 10^7 \ \frac{V}{m}$.

2.6.2 ITO

This substrate is purchased from Ossila Ltd. and it is a soda-lime float glass with a 20 nm coating of SiO_2 with a 20 x 15 x 1.1 mm dimension. On this glass are ITO electrodes with a height of 100 nm and an electrode width of 2 mm. The thickness of the stripes is 100 μm and the distance beween the electrodes is variable starting with the smallest with $d = 50$ μm, following with $d = 75$ μm, then $d = 100$ μm, next with

$d = 150\ \mu m$ and ending with the largest distance with $d = 200\ \mu m$.[Intb] This substrate with the variable spacing was chosen because when a voltage is applied, five different electric fields are obtained and thus more detailed investigations are possible. Since the distance between the electrodes is greater than for the gold electrodes, a higher voltage must be applied to obtain the same electric field, which was not possible with the voltage source used, since it is limited at 235 V. Unlike the gold substrate, there is no voltage limit for this substrate. Therefore the maximum electric field in the smallest gap is with eq. 2.12 $E = 4.7 * 10^6\ \frac{V}{m}$ and in the largest gap $E = 1.175 * 10^6\ \frac{V}{m}$

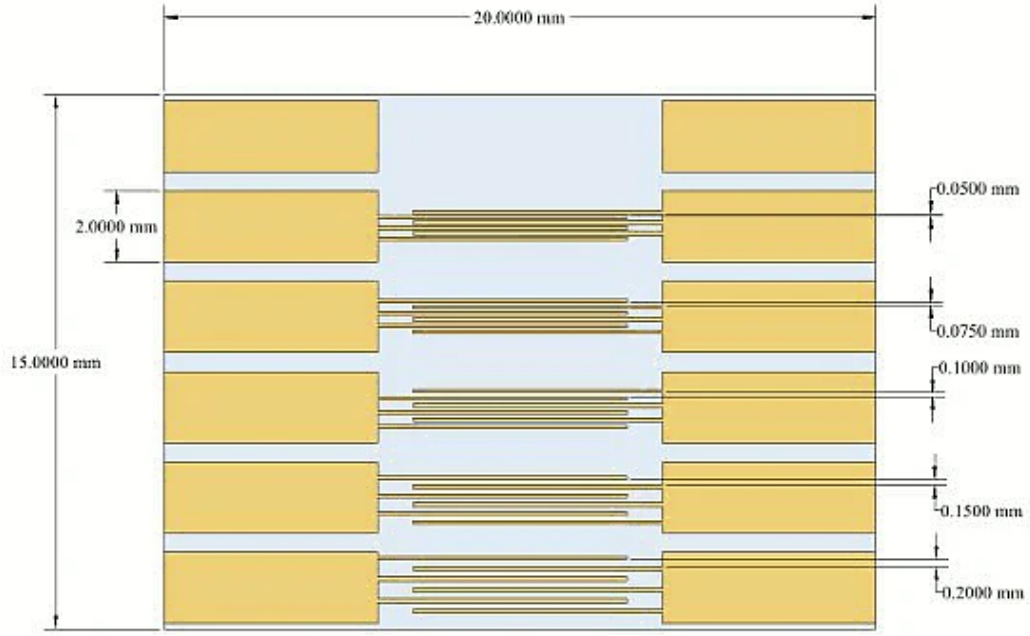

Figure 2.18: Shematical illustration of the glass substrate with ITO electrodes on it. The distance between the electrodes is variable with the smallest distance 50 μm and the largest distance 200 μm.[Intb]

3 Molecules

3.1 Molecules

In recent decades, there has been an increasing search for solution processable organic field effect transistor (OFET) materials for industrial use. Polymeric materials such as poly(3-hexylthiophene) (P3HT) have been investigated, but these are limited in their static distribution of molecule size and structural defects can acts as a carrier trap. Therefore, small molecule organic semiconductors (OSCs) are used due to the advantages such as the well-defined structure and ease of purification.[Eba+07] However, the use of OSCs has two deficits. First is the poor uniformity and rough surface morphology of solution processed films and second is the low melting point.[IUH15] [1]benzo-thieno[3,2 b]benzothiophene (BTBT) has demonstrated one of the highest mobilities reported so far. With its attractive core unit for structure-property relationship studies it also has multiple successful derivations such as 2-decyl-7-phenyl-[1] benzothieno[3,2-b][1] benzothiophene (Ph-BTBT-10) depicted in fig. 3.1.[Sch+15] Ph-BTBT-10 is an asymmetric molecule which has on one side of the aromatic BTBT core a phenyl ring and on the other side a decyl chain causing specific phase transitions at higher temperatures. Cooling from the smectic A phase at 223 °C to 210 °C the molecules undergo a transition to the smectic E phase.[Hof+21] The molecule Ph-BTBT-10 used in our experiments is a dry crystalline powder from the department of materials science of the University of Milano-Bicocca in Italy.

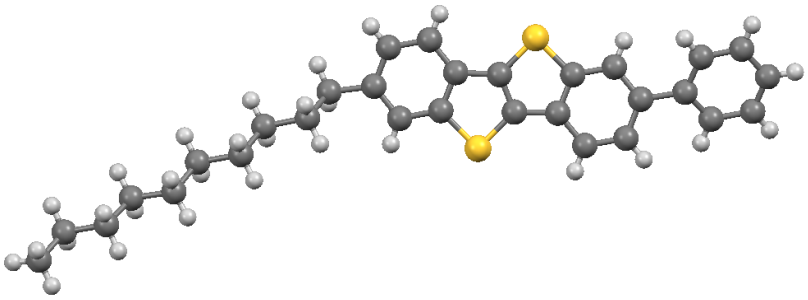

Figure 3.1: Chemical structure visulisation of Ph-BTBT-10 with Mercury. It consists of 30 carbon atoms (grey), 32 hydrogen atoms (light blue) and the core has two sulfur atoms (yellow).

Another derivative of the BTBT molecule is 2-decyl-7-phenyl-[1]benzothieno[3,2-b][1] benzothiophene S,S,S',S'-tetraoxide (Ph-BTBTOx_2) depicted in fig. 3.2. This molecule is formed by the transition from p-type to n-type transistor in BTBT-like structures

during the oxidation of sulfur atoms. Thus, Ph-BTBTOx$_2$ is synthesized directly from Ph-BTBT-10 by oxidation with m-chloroperbenzoic acid in a dichloromethane solution. It has three different stable phases, while the first is at room temperature, the second is at 95 °C and the last is at 135 °C. At room temperature, this molecule has a disordered phase that undergoes two phase transitions to reach ordered crystallinity at 135 °C. The first phase transition is at 95 °C, resulting in a defined out-of-plane structure but no in-plane ordering. The second phase transition is, of course, at 135 °C, at which the mobility of the molecules is high enough for crystallization. [Bod+20]

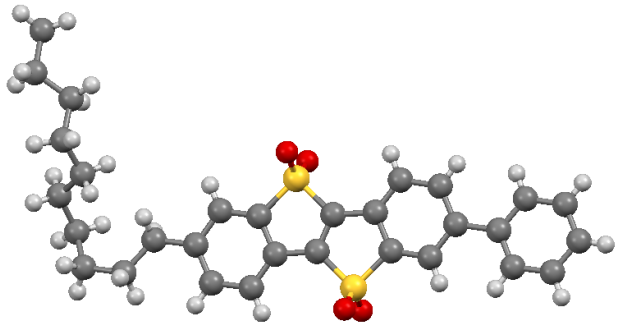

Figure 3.2: Chemical structure of Ph-BTBTOx_2. On the right is the aromatic BTBT core and on the left is its extension to this derivative. It consists of 30 carbon atoms (grey), 32 hydrogen atoms (light blue) and the core has two sulfur atoms (yellow) plus additional four oxygen atoms (red).

Another molecule used in this thesis is α-quinquethiophene depicted in fig. 3.3 and it is another small molecule organic field effect transistor with a high field effect mobility [Haj+97] and a high melting point at 253 °C [Qqp]. Thiophene and its derivatives contribute a significant amount of the organosulfur compounds formed in petroleum as well as in some other fossil fuel products. Thiophenes are heterocyclic aromatic compounds based on a five-membered ring consisting of one sulfur and four carbon atoms while quinquethiophene has five of this rings coupled together with their α carbons. [Ibr+16] The molecule quinquethiophene used in this experiments was orderd from Sigma Aldrich and was delivered in an powder form with a purity of 95 % .

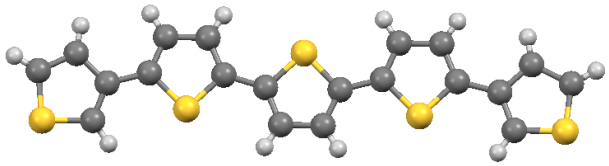

Figure 3.3: Chemical structure of Quinquethiophene. It consists of 20 carbon atoms (grey), 12 hydrogen atoms (light blue) and five sulfur atoms (yellow).

All three molecules have a small dipole moment, while the dipole moments of the two BTBT derivatives are unknown. Quinquethiophenes dipole moment is 1.47 D (1 D =

$3.33564 * 10^{-30}\ Cm$).[Vás08] To orientate a single molecule in an electric field its potential energy (E_{pot}) must be higher than its kinetic energy (E_{kin}). The kinetic energy of the molecules in room temperature is calculated with eq. 1.6 and is approximately $4 * 10^{-21} J$. Thus, the potential energy, described by eq. 1.5, must be greater than $4 * 10^{-21} J$. For our experiments with a maximum electric field of $E = 1.8 * 10^7\ \frac{V}{m}$ at least a dipole moment of 200 D is needed. In a vapor growth experiment (PVD), the electric field acts on the molecules migrating on the surface or on the growing crystals and not with the free molecules. Often the interaction with the substrate is larger than with the electric field and thus the effect of the electric field has an effect only on small grain sizes even if the electric field would be large enough. In contrast, in a solvent-based process, the molecules are more mobile and interact better with the electric field, allowing them an alignment along it even at lower field strengths.[KOS16]

4 Results and Discussion

First, the gold and ITO substrates are cleaned with acetone by placing the samples in an acetone bath for two minutes. The substrates are then rinsed with acetone, followed by another rinse with 2-propanol, and then dried with a carbon dioxide pressurized gas bottle. After cleaning, the PVD experiment can be started, where two substrates of one type are placed into the vakumm chamber ($p = 3.2 * 10^{-6}\ mbar$). One substrate is without voltage and the voltage on the other substrate is changed for each experiment to evaluate the influence of the electric field. The voltage on the gold substrate is between 130 V and 180 V and on the ITO substrate 235 V. The heating target for the Ph-BTBT-10 molecule is the Knudsen cell and for the Ph-BTBTOx_2 and the quinquethiophene molecule the tungsten boat is used. The average evaporation time, this means from beginning of heating up till switching off the power supply, to reach a film thickness of 20 nm, is 15 min. After evaporation, images are taken first with the optical microscope and then with the atomic force microscope. When measuring with the AFM the images for every sample are taken with a resolution of 512 pixels and a scanning speed of 1 second per line, which corresponds to a measurment duration of about 20 min. Following the AFM measurement the XRR measurements are performed. The experimental setup uses a 1/32 divergence slit, a 4 mm beam mask and a 0.1 mm anti-scatter slit and the diffraction pattern is measured for 1 hour. The x-axis is converted to the scattering vector q using eq. 2.7 to obtain a wavelength-independent measurement. After measurements are done, the solvent vapor annealing experiment is performed for 4 hours. The chosen solvents are chloroform and toluene. Most experiments are performed with chloroform because better results are obtained than with toluene. As in the PVD experiment one substrate is again without a voltage and on the other substrate the voltage is between 12 V and 30 V for the gold substrate and between 150 V and 180 V for the ITO substrate. When the solvent vapor annealing experiment is finished, the samples are measured again with the optical microscope, the AFM and the Panalytical diffractometer. The substrates were further measured after PVD as well as after SVA with GIXD to obtain more accurate information on the orientation of the molecules. Since the time window for the use of the synchotron was only one weekend, not all required samples could be measured. In addition most of the experiments are done on the gold substrate, because the electrodes are closer to each other resulting in a higher electric field.
In Fig. 4.1 the optical microskop picture of the clean gold substrate with fivefold magnification is depicted and in fig. 4.2 the same substrate with hundredfold magnification is shown.

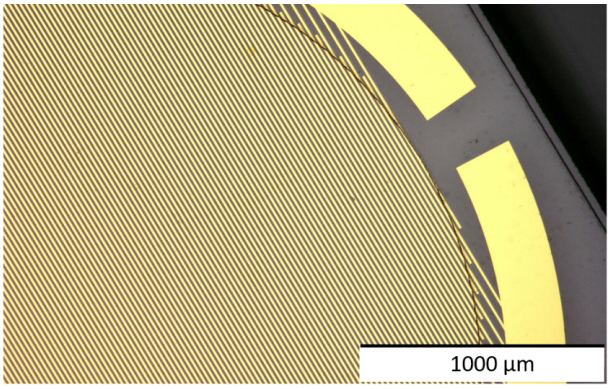

Figure 4.1: Optical microscope image of the upper electroctrode area of the Au-substrate with fivefold magnification

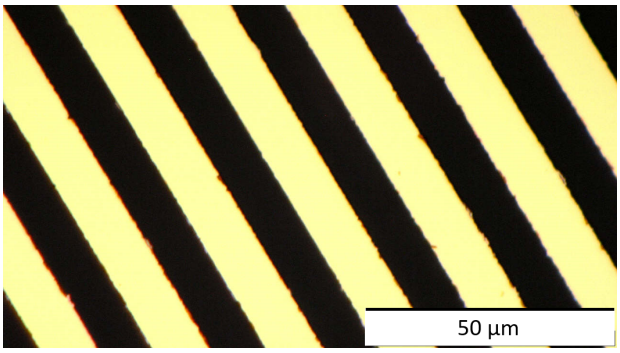

Figure 4.2: Optical microscope image of the cleaned Au-substrate with hundredfold magnification

Fig. 4.3 shows the atomic microscope image of the cleaned substrate. The height of the electrodes, the width of the electrodes and the distance between them is measured with the AFM. The measurements agree with the data from the manufacturer and are 150 nm for the height and 10 μm for the width of the electrodes as for the distance between them. The optical microscope as well as the AFM images of the molecules on the ITO substrate does not provide any usable results so there is no need for the images of the cleaned substrate.

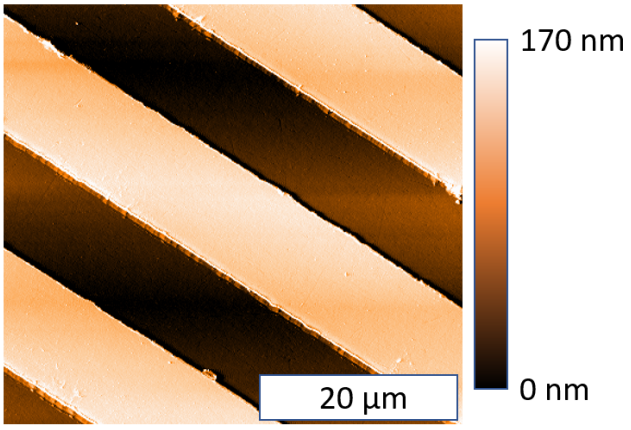

Figure 4.3: Atomic force microscope image of the cleaned Au-substrate

Fig. 4.4 shows the difraction pattern of the cleaned substrate. Two critical angles are visible, the first is from the glass substrate and the second is from the gold. The small Kiessig fringes are from the SiO_2. The results to the experimental data are described and discussed in the following chapters.

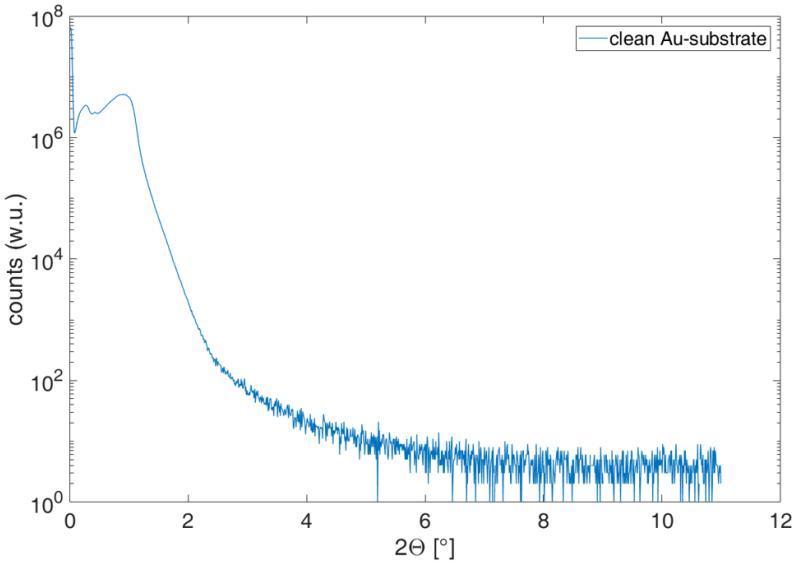

Figure 4.4: XRR measurement of the cleaned Au-substrate showing two critical angles corresponding to the SiO_2 substrate and to the gold electrodes.

4.1 Ph-BTBT-10

4.1.1 Optical microscope

Fig. 4.5 shows an optical microscope image of Ph-BTBT-10 of two Au-substrates at the same experiment run with a film thickness of 18 nm at a fivefold magnification. The left sample is voltage free and the right sample has a voltage of 160 V on the electrodes. The black dots in the left picture are the Ph-BTBT-10 crystals. The substrate to which a voltage is applied, show a lower crystal denisty as the the voltage-free substrate in the optical microscope image. The same effect appears when appling an external electric field on the crystallization of proteins. [Tal+99]

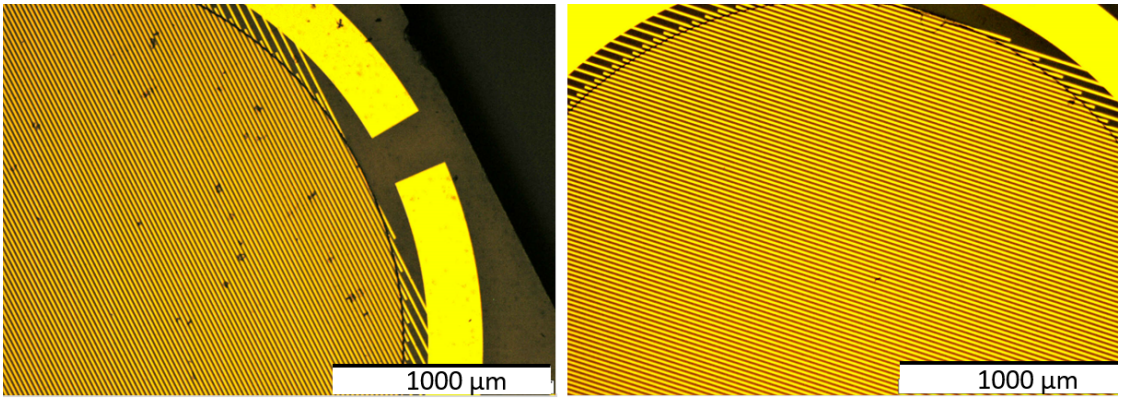

Figure 4.5: Both images are from the same physical vapor deposition experiment of Ph-BTBT-10 on the Au-substrate. The left substrate has no voltage and the right substrate has a voltage of 160 V.

As explained in the introduction, an electric field has an influence on various properties in a crystallization process. In this comparison, it is clear that the electric field has an influence on the nucleation density. However, as claimed in the article by Lee Fiona Alexander and Norbert Radacsi [AR19], neither the orientation nor the reduction of the nucleation time can be detected with an optical microscope. Also, since the electrodes are too close together, the difference in crystal size between the substrate with and without voltage cannot be determined with the optical microscope as well.

Following the PVD experiment, the substrates are solvent vapor annealed. Fig. 4.6 shows the image of an optical microscope of the SVA samples at five times magnification. The left substrate is treated without voltage supply and the right substrate is treated with a voltage of 20 V on the electrodes. The effect of a lower crystal density when an electric field is applied, as in the PVD experiment, cannot be seen here because the molecule is on the substrate already before this treatment. In the upper left part of the right image, dewetting occurs due to the solvent, which is why more molecules are found in this area. Dewetting is a thermodynamic process and describes the accumulation of a liquid film into three-dimensional islands. [Ler+16] This dewetting and subsequent crystallization occurs at random locations on the substrate and is hard to control. Fur-

thermore, it is apparent that the agglomeration of molecules on the positive anodes is larger because the electrodes are darker there.

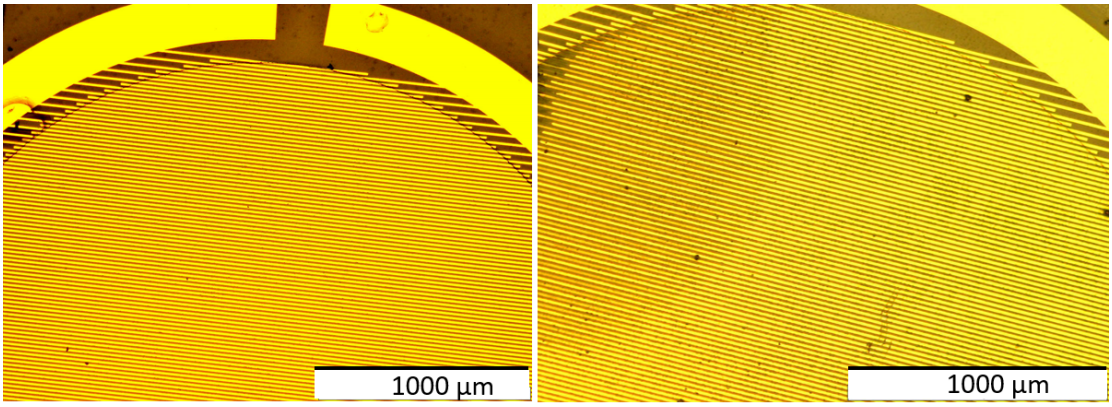

Figure 4.6: Both images are from the same solvent vapor annealing experiment of Ph-BTBT-10 on the Au-substrate at a fivefold magnitude. Both samples have a film thickness of 30 nm. The left sample is treated without voltage and the right sample is treated with a voltage of 20 V.

If these areas are viewed at a higher magnification as depicted in fig. 4.7, where the substrate without voltage is on the left and the substrate with 20 V is on the right, this effect becomes more visible. The molecules move from the negative electrode to the corner of the positive electrode. A possibility for this is that the molecules are negatively charged during the SVA process. The transformation into a negatively charged molecule is also called deprotonation which means the removal of a proton. As the samples are stored in ambient conditions after the PVD experiment, a water film can form on the surface of the substrate. The water, in turn, acts as a proton acceptor, causing the molecule to become negatively charged.[Vel+17]

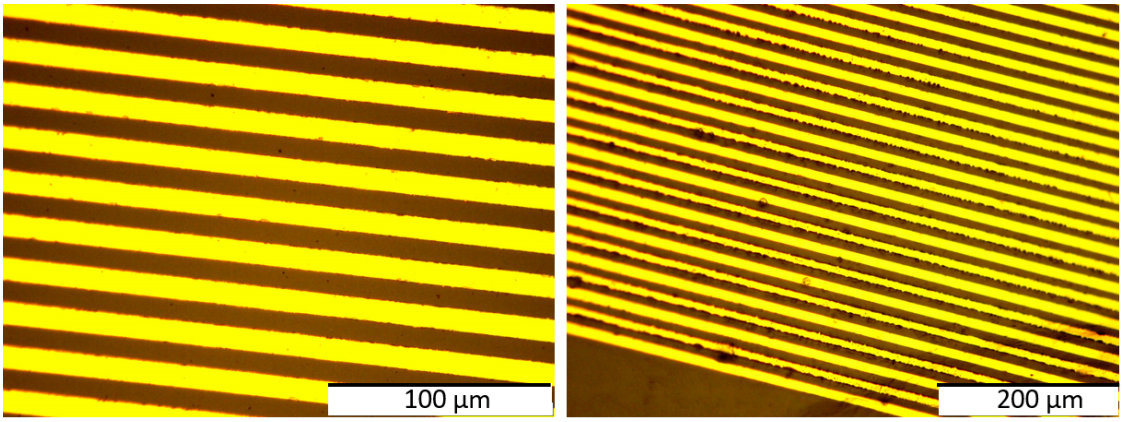

Figure 4.7: Both images are from the same solvent vapor annealing experiment of Ph-BTBT-10 on the Au-substrate while the left has a magnitude of 50 and the right has a magnitude of 20. The left sample is treated without voltage and the right sample is treated with a voltage of 20 V.

4.1.2 Atomic force microscope

Since the optical microscope image in fig. 4.5 after PVD shows a different number of nucleation sites, but no other influences of the electric field, the substrates are measured even more precisely by atomic force microscopy. Depicted in fig. 4.8 are the gold substrates after the PVD experiment with a film thickness of 21 nm, where the gap between the electrodes is in the middle and the electrodes are in the left bottom corner and right top corner. The left is the substrate with no voltage and the right is the substrate with a voltage of 130 V. The density of nucleation nuclei is higher on the substrate without voltage than on the substrate with voltage, as already seen in the optical microscope image. Furthermore, in the left image, the accumulation of molecules at the corner of the right electrode is larger than at the corner of the left electrode. This is not the case for the substrate with voltage applied. Since the AFM measures in one direction, i.e. the measuring head moves the sample in one direction and does not measure the sample when moving back, it can be an error of the measurement. In addition, the right image shows larger crystals than the left image, but with only two such crystals, it is not possible to make a statement about the influence of the electric field on the crystal size. Also, the influence on the orientation and growth along the electric field cannot be observed, as the electric field is probably to weak. However, another effect becomes apparent when the height of the electrodes is measured. Thus, for the substrate without voltage, the height difference between electrode and substrate is 150 nm, and for the substrate with voltage, it is 165 nm. This means that the molecule Ph-BTBT-10 condenses more on the electrodes with voltage on both the positive and negative electrodes. Due to the fact that the electric field is only between the electrodes and not on top of the electrodes, it could be that the condensation between the electrodes is reduced as a result of the electric field. Thus, in the PVD experiment, the molecules condense almost only at the

electrodes when voltage is applied.

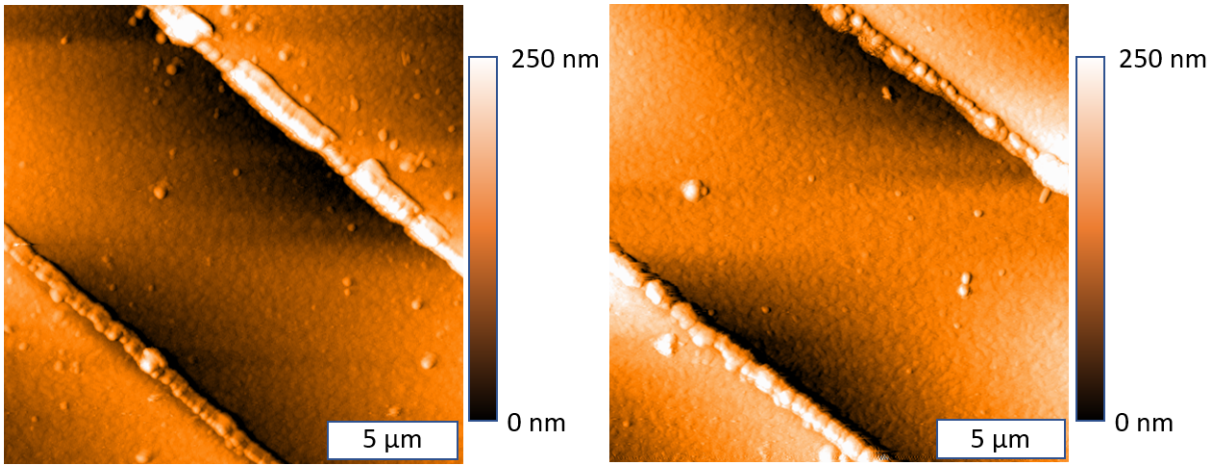

Figure 4.8: Both AFM images are from the same PVD experiment where on the left substrate no voltage is applied and the right image is of the substrate with 130 V

The gold substrates with a Ph-BTBT-10 film thickness of 29 nm are depicted in fig. 4.9 after solvent vapor annealing. The left image is the voltageless substrate and the rigth image is the substrate with 20 V. In the case of the left substrate, after annealing only the density of individual crystals decreased, but the accumulation of molecules at one electrode remained unchanged, which again suggests an error in the measurement. On the right substrate, in turn valley formation occurs. This means that there is a thinner fim next to the negative electrode (second from right) than next to the positive electrodes (second from left and first from right). This indicates that the molecules migrate to the positive electrode during the SVA process and accumulate there. Thus, almost all particles are at the positive electrodes, which can also be confirmed with the height difference measurement. Unfortunately, no growth in the direction of the electric field nor the orientation of the molecules can be determined with the AFM for this molecule after the SVA process.

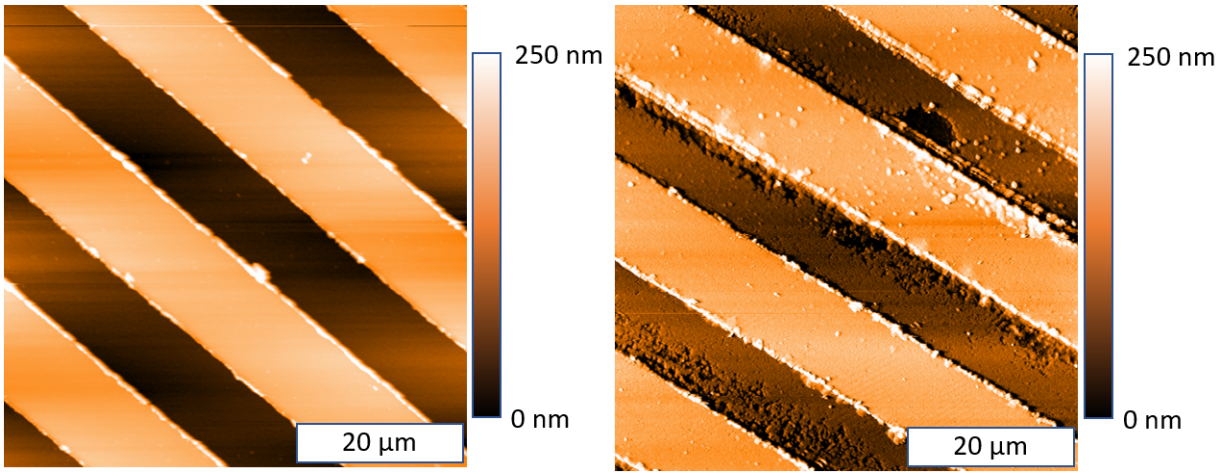

Figure 4.9: Both AFM images are from the same SVA experiment where on the left substrate no voltage is applied and the right substrate has a voltage of U = 20 V.

4.1.3 X-ray reflectivity

For the characterization and determination of the orientation of the molecule specular x-ray diffraction measurements are performed. In fig. 4.10 the resulting measured diffraction pattern of Ph-BTBT-10 on the gold substrate after PVD and after SVA is shown. The diffraction pattern shows defined diffraction peaks for all three spectra, although those after PVD differ with those after SVA. These peaks can be identified based on the known crystal structure of Ph-BTBT-10, where the first peak at 0.118 $\mathring{A}^{-1}$ is the 001 Bragg peak and the others are higher order reflections, i.e., the second peak 002 is at $q = 0.236\mathring{A}^{-1}$, the third 003 is at $q = 0.354\mathring{A}^{-1}$, and the fourth peak 004 is at $q = 0.472\mathring{A}^{-1}$. There is no difference in the samples after PVD except of a broader peak by the sample with a voltage of 160 V, confirming that the electric field used in the PVD experiment is too low. The broader peak can have two reasons. First, because of microstrains or second, because of the crystal size.[Hof+21] The latter is more likely because the film thickness at the substrate with voltage is 29 nm and the film thickness at the substrate without voltage is 18 nm. For the substrate after the SVA, two additional peaks are visible at $q = 0.118\mathring{A}^{-1}$ and $q = 0.354\mathring{A}^{-1}$. The reason for this could be the smoothing due to the chloroform, since these peaks also occur in the paper by Hofer when using chlorobenzene.[Hof+21] Based on the fact that only the peak 001 and its higher orders can be seen in the specular diffraction pattern, it can be assumed that there is a strong out-of-plane preferential orientation of the crystallites. As a result, the crystals in our case grow with the (001) plane parallel to the surface of the substrate after the PVD experiment and after the SVA experiment.

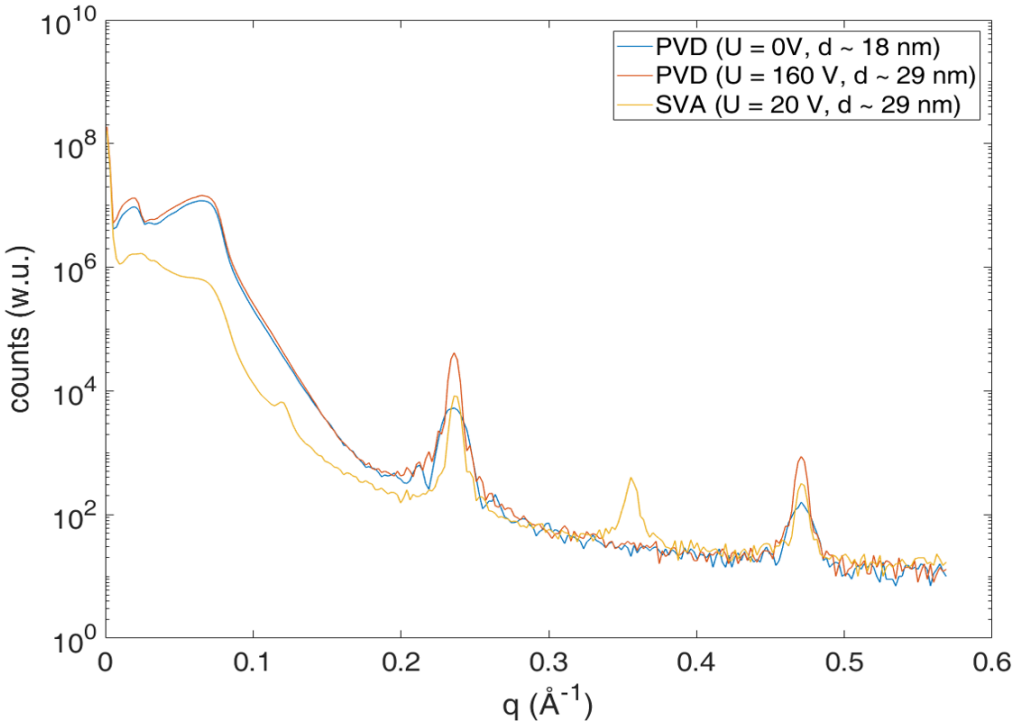

Figure 4.10: XRR pattern of Ph-BTBT-10 after PVD at 0 V (blue) 160 V (red) and after SVA at 20 V (orange)

In this measurement, the influence of the electric field on the orientation of the crystals could not be shown. The molecules could be oriented in-plane, which is not possible to measure, because only the out-of-plane orientation is detected in the XRR measurement.

4.1.4 Grazing incidence x-ray diffraction

To obtain more precise information on the orientation of the molecules on the gold substrate, an extended range GIXD pattern was measured. The incoming beam hit the substrate at an angle of 0.5° and the sample was rotated by 180° to measure the in-plane orientation as well. The measurement of the diffraction pattern is converted with the program GIDVis into the reciprocal space, where afterwards the peak positions and the peak intensities are analyzed. The ITO substrates were also measured but could not provide any information. Fig. 4.11 shows the reciprocal space map of Ph-BTBT-10 on the Au-substrate after PVD with indexation with the known crystal structure assuming the 001 orientation. The bright peaks on the left edge are from the gold electrodes as well as the bright ring in the middle. The agreement of the intense peaks (111, 112, 115, 002 and 020) with the theoretical points are the evidence of the known crystal structure of Ph-BTBT-10. To analyze the in-plane orientation, the intensity of a strong peak at each rotation is summed up and plotted in a graph. The starting postion of the sample before rotating is that the gold electrodes are parallel to the incoming beam.

This means that after a 90° rotation, the electric field between the electrodes is parallel to the incident beam, where the intensity of the peak should be highest if the crystals are oriented along the field.

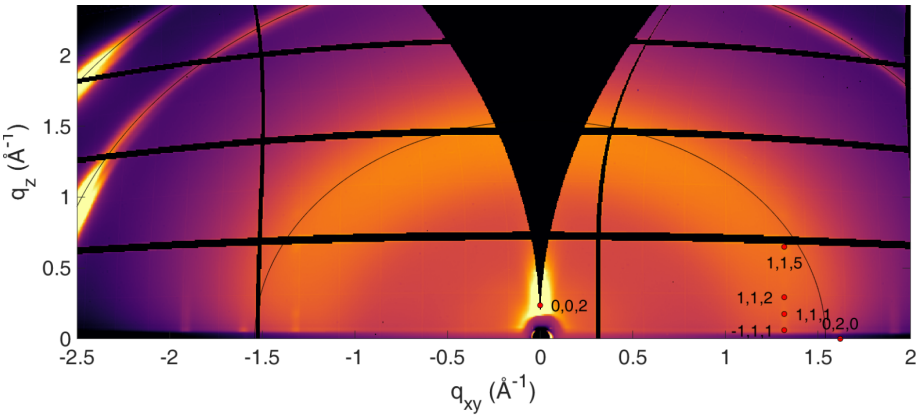

Figure 4.11: GIXD-Map of Ph-BTBT-10 on the gold substrate after physical vapor deposition

Fig. 4.12 shows the dependence of the intensity of the 111 peak on the rotation of the substrate after the PVD experiment with a voltage of 160 V. The sample is rotated 360° in one degree increments and it does not show any large change in intensity between 0°, 90°, 180°, 270° and 360°, demonstrated with the black line, which means that there is a weak in-plane orientation after PVD.

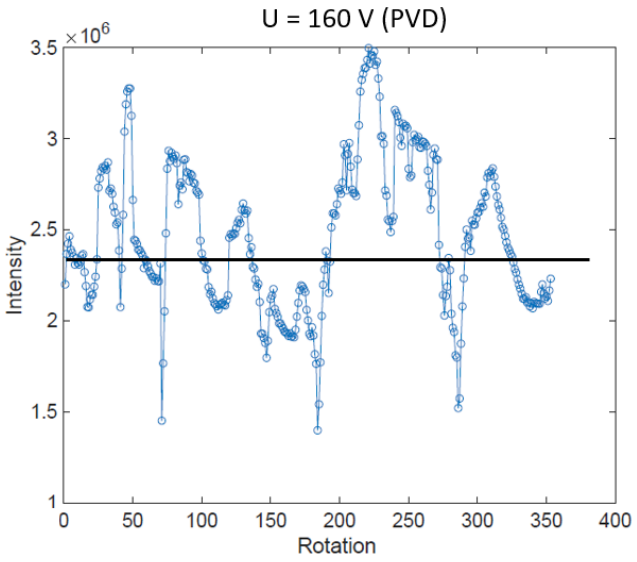

Figure 4.12: Intensity of the 111 peak from the 360° rotated Au-sample after the physical vapor deposition experiment with a y-axis of 10^{-6}.

Fig. 4.13 shows the dependence of the intensity of the 111 peak on the rotation of the substrate after the SVA experiment with a voltage of 20 V. The substrate is rotated 180° in two degree increments, which means that by an rotation of 45 we have an actual rotation of 90°. This sample, in turn, has an intensity drop around the 90° rotation, illustrated with the two black lines, which means that the molecules are oriented in the direction of the gold electrode and not in the direction of the electric field. Thus, the orientation is more influenced by the substrate and less by the electric field.

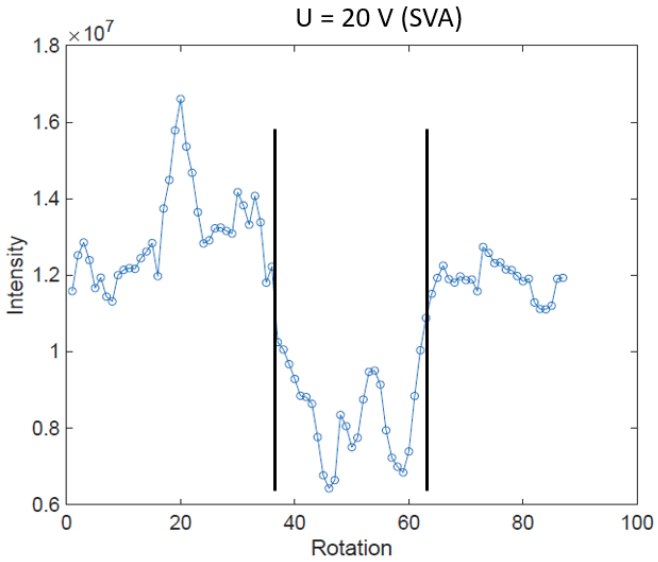

Figure 4.13: Intensity of the 111 peak from the 180 ° rotated Au-sample after the solvent vapor annealing experiment with a y-axis of 10^{-7}.

4.2 Ph-BTBTOx$_2$

4.2.1 Optical microscope

Fig. 4.14 shows the two gold substrates after PVD experiment with Ph-BTBTOx$_2$ with a film thickness of 16 nm, where on the left is the substrate without voltage and on the rigth is the substrate with voltage of 160 V. In principle, the Ph-BTBT-Ox$_2$ molecule shows the same behavior in the PVD experiment as Ph-BTBT-10. For the substrate with applied voltage the amount of the crystals is lower than for the substrate without applied voltage. The yellow stripes are the gold electrodes and the black dots are the Ph-BTBTOx$_2$ crystals. However, no further information about the influence of the electric field on crystallization is obtained with the light microscope images for this molecule either.

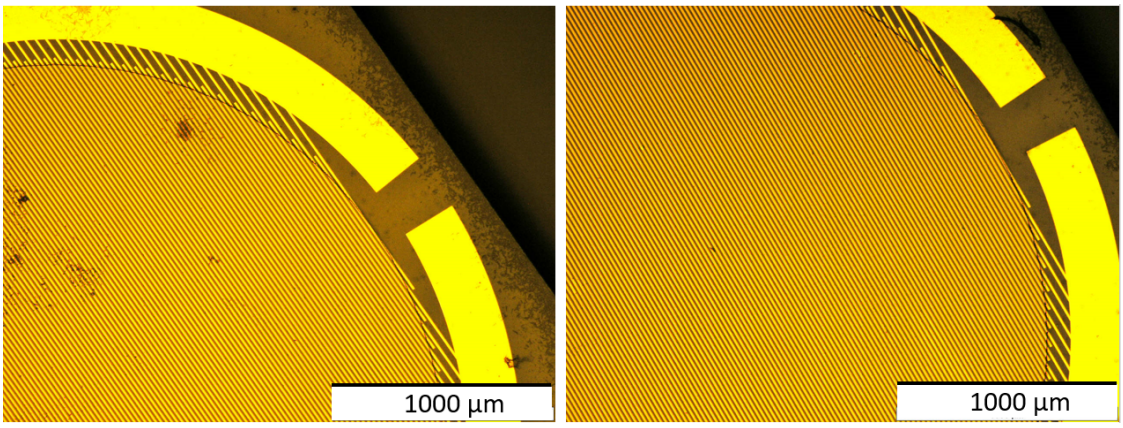

Figure 4.14: Both images are from the same physical vapor deposition experiment of Ph-BTBTOx$_2$ on the Au-substrate where the left substrate has no voltage and the right substrate has a voltage of 160 V.

After solvent vapor annealing, the PVD samples are measured again with the optical microscope. In fig. 4.15, the substrate without voltage is shown on the left and the substrate with an applied voltage of 20 V on the right. In the case of the substrate without voltage, the film becomes smoother after treatment, and in the case of the substrate with voltage, the molecules collect at the positive electrode. It seems that this molecule also becomes negatively charged due to deprotonation and therefore migrates to the positive electrodes.

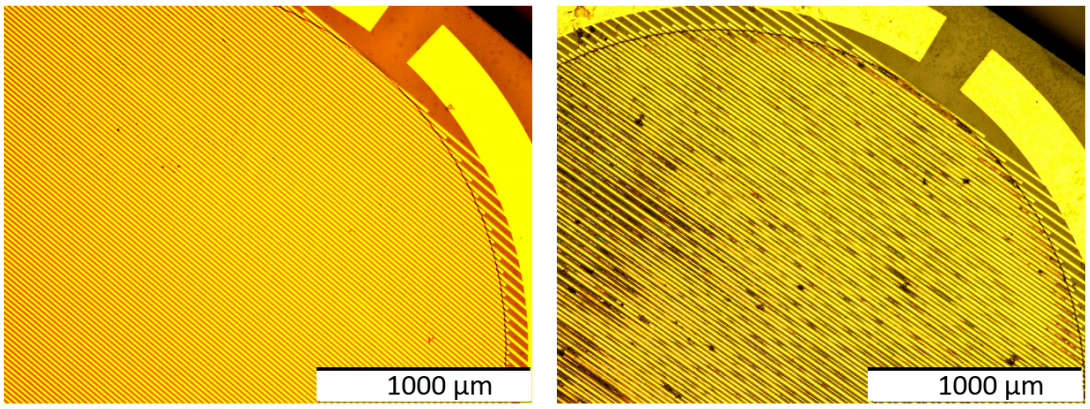

Figure 4.15: Both images with a fivefold magnification are from the same solvent vapor annealing experiment of Ph-BTBTOx$_2$ on the Au-substrate with a film thickness of 16 mn. The left substrate has no voltage and the right substrate has a voltage of 20 V.

When the substrate with voltage applied is viewed at a magnification of twenty times, as in the left image of Fig. 4.16, the accumulation at the positive electrodes is more visible. This accumulation is not only at the edges of the electrodes but also on top of them. In the right picture the substrate is illuminated from below with an fiftyfold magnification. In this case the black stripes are the gold electrodes and the white stripes are from the substrate between the electrodes. Between the electrodes there is a rod-like growth along the electric field, as it is also described in the article of Kotsuki.[KOS16] This growth may be due to the electric field, but it may also be due to defects in the gold electrodes. In the later case, a nucleation site aligned perpendicular to the gold electrode is formed at a defect location in the gold electrode. Subsequently, this nucleus grows and forms this rod-like structure. However, since this growth is not seen in PVD and is often seen in SVA, the second case is quite unlikely.

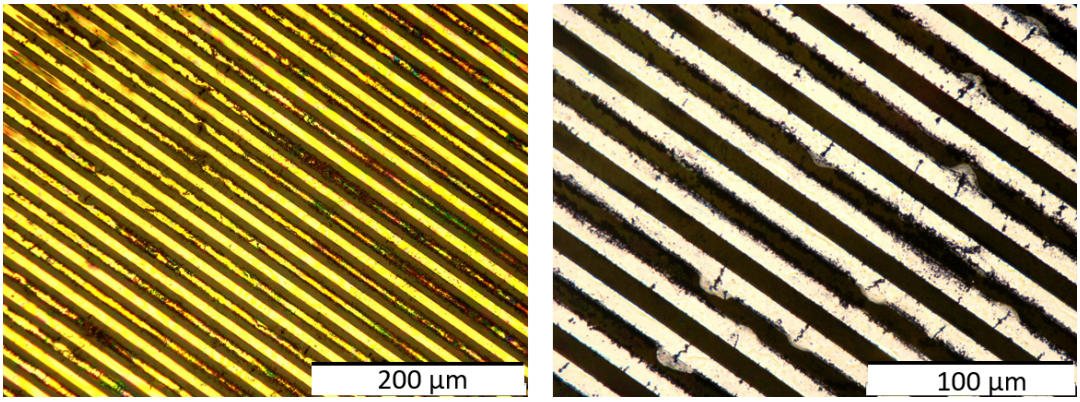

Figure 4.16: The left image is a twentyfold magnification from the SVA experiment of Ph-BTBTOx$_2$ on the Au-substrate. The right image is a negativ image, where the specimen is illuminated from below. On the negativ image rodlike structures along the electric field are visible.

4.2.2 Atomic force microscope

Fig. 4.17 shows the two gold substrates after PVD experiment with Ph-BTBTOx$_2$ with a film thickness of 28 nm, where on the left is the substrate without voltage and on the rigth is the substrate with voltage of 150 V. For both substrates, as with the previous molecule, the collection is again at one corner of the electrodes, but at opposite sides. The reason for this could be that the running direction of the measurement was changed because the substrates were not measured on the same day. As in the evaluation with the optical microscope, it can be seen that the density of the nucleation sites is greater on the substrate without voltage than on the substrate with voltage. Furthermore for this molecule, it is also visible that the crystal size is larger on the substrate with electric field than on the other as it is claimed in theory.[AR19] As with Ph-BTBT-10, when measuring the height difference, the difference is greater at the substrate with applied voltage. For the substrate without voltage the difference in height between electrode and substrate is 155 nm and for the substrate with voltage it is 175 nm. As in the Ph-BTBT-10 molecule if a voltage on the substrate is applied, also the Ph-BTBTOx$_2$ condesates mostly on the electrodes.

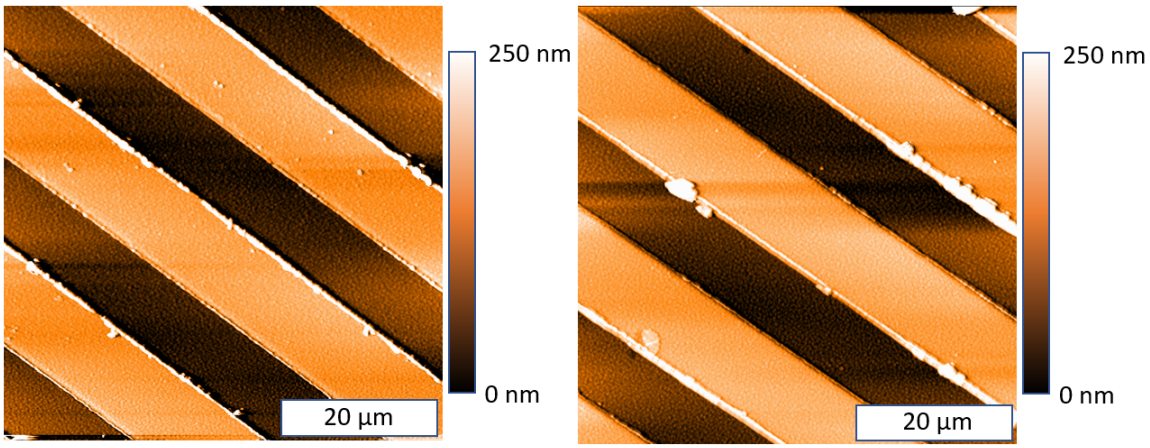

Figure 4.17: Both AFM images are from the same PVD experiment, where on the left substrate no voltage is applied and it has about 24 nucleation sites and the right image is of the substrate with 150 V with about 13 nucleation sites.

Fig. 4.18 shows the substrates with a film thickness of 20 nm after solvent vapor annealing where the left image is the substrate treated without voltage and the right image is the substrate treated with a voltage of 20 V. If no voltage is applied to the substrate, a smoothing of the surface can be seen as well as again a deposition at one electrode corner (left picture). If a voltage is applied during the experiment, the molecules migrate to the positive electrode (right image). Even though the growth along the electric field was visible with the optical microscope, this spicific location was not found with the AFM.

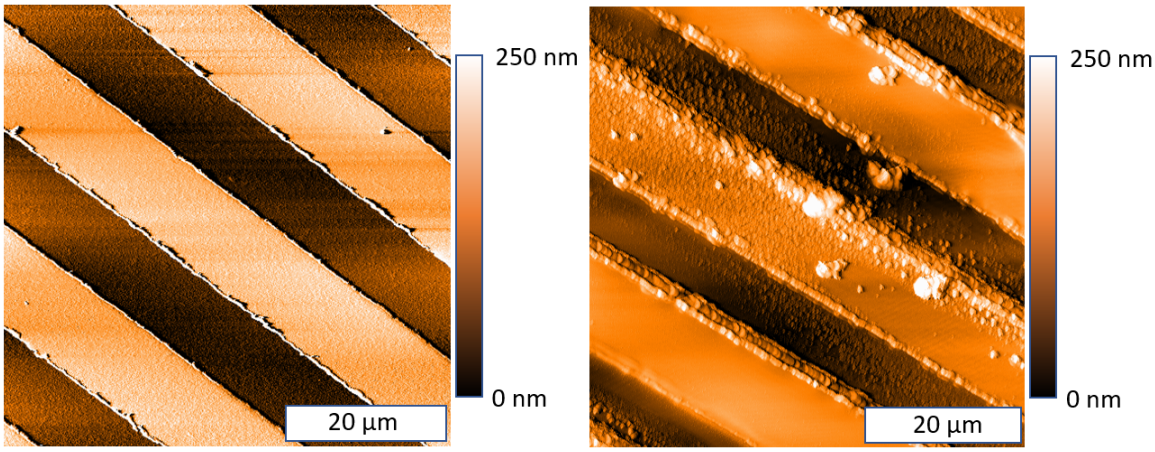

Figure 4.18: Both AFM images are from the same SVA experiment where the left substrate is treated without voltage and the right substrate is treated with a voltage of U = 20 V.

4.2.3 X-ray reflectivity

Fig. 4.19 shows the diffraction pattern of the molecule after PVD and after SVA, each with a substrate with and without voltage. Thereby, after the PVD experiment at $q = 0.474\mathring{A}$, the 001 Bragg peak for the known crystal structure is seen for both the substrate with and without voltage, showing that the electric field has no effect on the orientation. After the SVA experiment, for the sample without voltage, no peak is visible. This sample was calibrated and measured several times to exclude a wrong alignment of the sample, but the same pattern was still measured. In the sample with voltage the peak is shifted and can be seen at $q = 0.415\mathring{A}$. This shift infers a new phase whose crystal structure is not known.

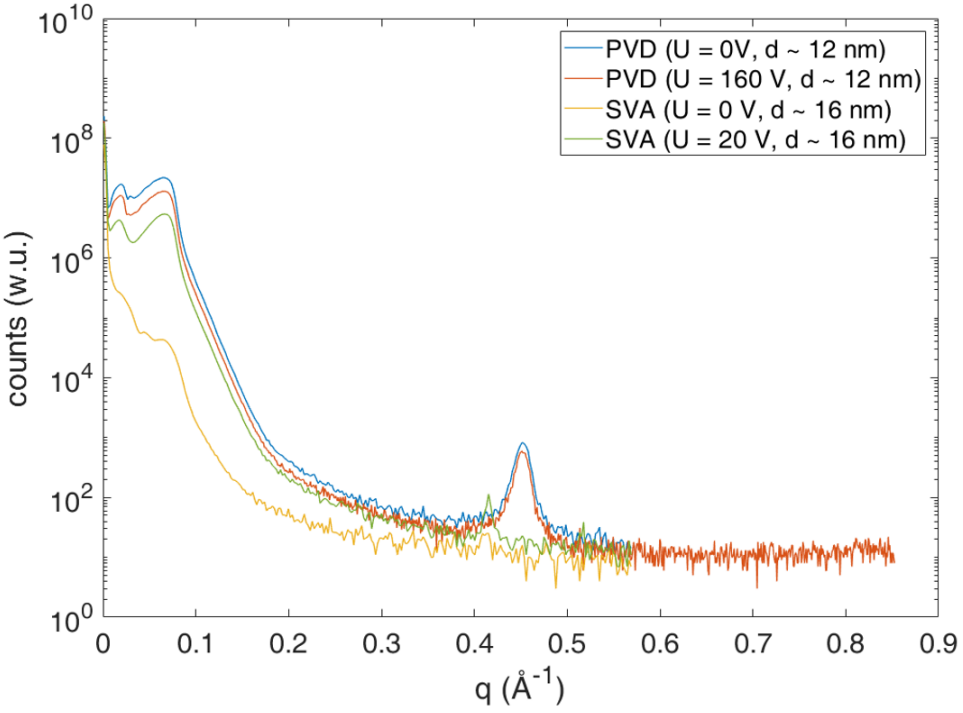

Figure 4.19: XRR pattern of Ph-BTBTOx$_2$ after PVD at 0 V (blue) and 160 V (red) and after SVA at 0 V (orange) and 20 V (green)

While only the peak 001 is visible in the specular diffraction pattern, it can be assumed that there is an out-of-plane preferential orientation of the crystallites. As a result, the crystals grow with the (001) plane parallel to the surface of the substrate after the PVD experiment and also after the SVA experiment.

4.2.4 Grazing incidence x-ray diffraction

Fig. 4.20 shows an extended range GIXD pattern of Ph-BTBTOx$_2$ on the Au-substrate. The incoming beam hit the substrate at an angle of 0.5° and for the determination of the

in-plane orientation the sample was rotated by 180°. The measurement of the diffraction pattern is converted with the program GIDVis into the reciprocal space, to evaluate the measurement. Unfortunately by measuring Ph-BTBTOx$_2$ just the 001 peak and the 002 peak and the peaks from the gold electrodes are visible and so no evaluation of in-plane orientation is possible.

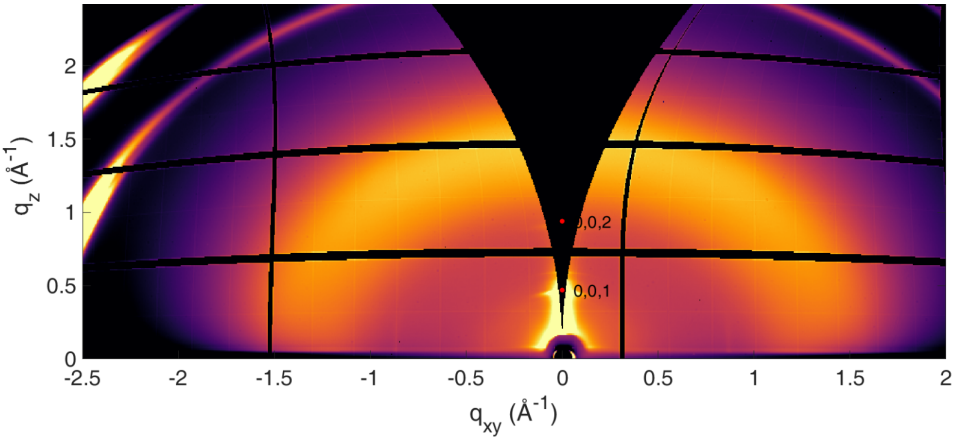

Figure 4.20: GIXD-Map of Ph-BTBTOx$_2$ on the gold substrate

4.3 Quinquethiophene

4.3.1 Optical microscope

In fig. 4.21 the optical microscope image from the Au-substrates after PVD with quinquethiophene are shown, where on the left substrate no voltage is applied and the right substrate has a voltage of 160 V. The black dots are again the crystals of the molecule and the yellow stripes are the interdigitated electrodes. As with the other molecules, a smaller nucleation density is seen on the substrate with voltage, but not as much as with the others.

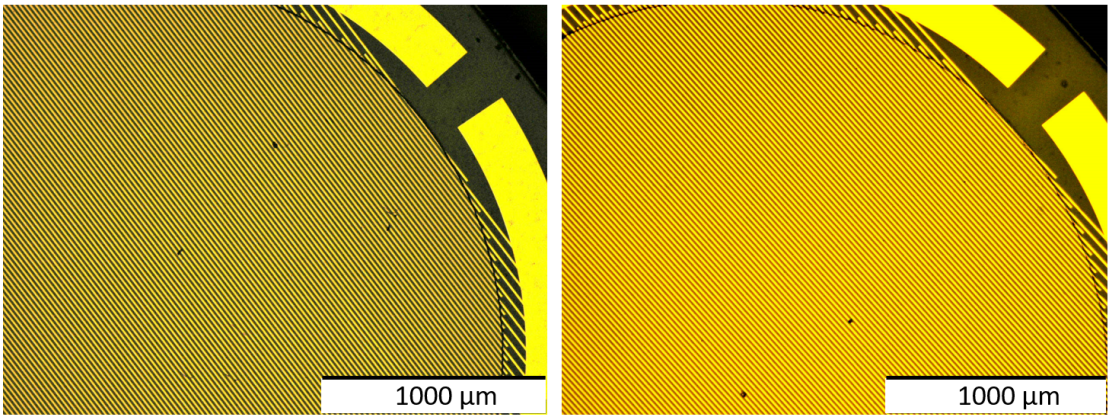

Figure 4.21: Both images are from the same PVD experiment of quinquethiophene on the Au-substrate. The left substrate has no voltage and the right substrate has a voltage of 160 V.

In the SVA experiment, the same behavior appears as for the other molecules, namely the attachment to the positive electrodes. Fig. 4.22 shows the fivefold magnification of the substrate without voltage (left image) and with a voltage of 20 V (right image). On the substrate with voltage, each positive electrode is completely covered. The reason for this could be the larger film thickness, which is 45 nm and thus twice as large as for the other molecules.

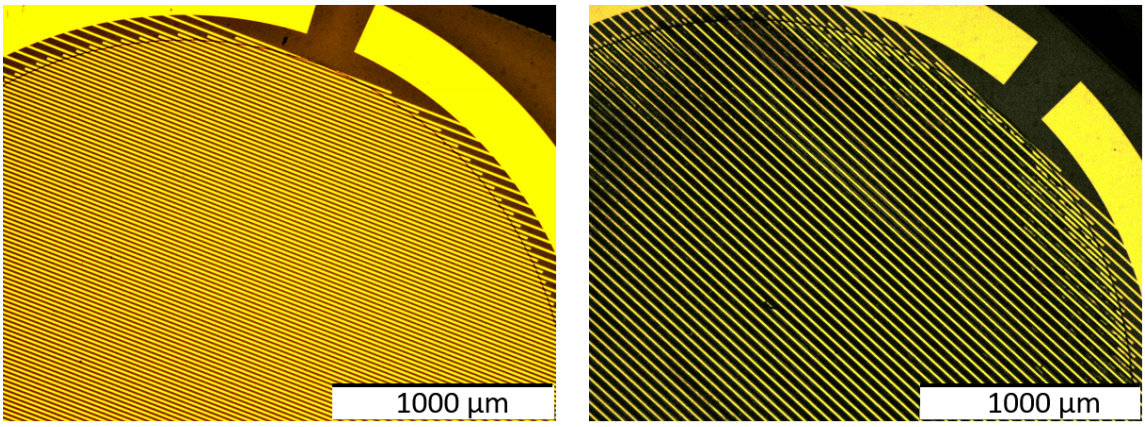

Figure 4.22: Optical microscope image of the fivefold magnification from the same SVA experiment of quinquethiophene on the Au-substrate. The left substrate is treated without voltage and the right substrate is treated with a voltage of 20 V.

Fig. 4.23 shows the fifty-fold magnification of the substrate without voltage (left image) and with 20 V (right image). In the case of the substrate with voltage, in addition to the deposition on the electrodes, structures can be seen between the electrodes, which, however, appear to be random. They do not grow rod-like in the direction of the electric field, as in the case of Ph-BTBTOx$_2$, nor do they grow rod-like in any other direction. It looks like there is an orientation in the direction of the electric field, but with the optical microscope images no further conclusions can be made.

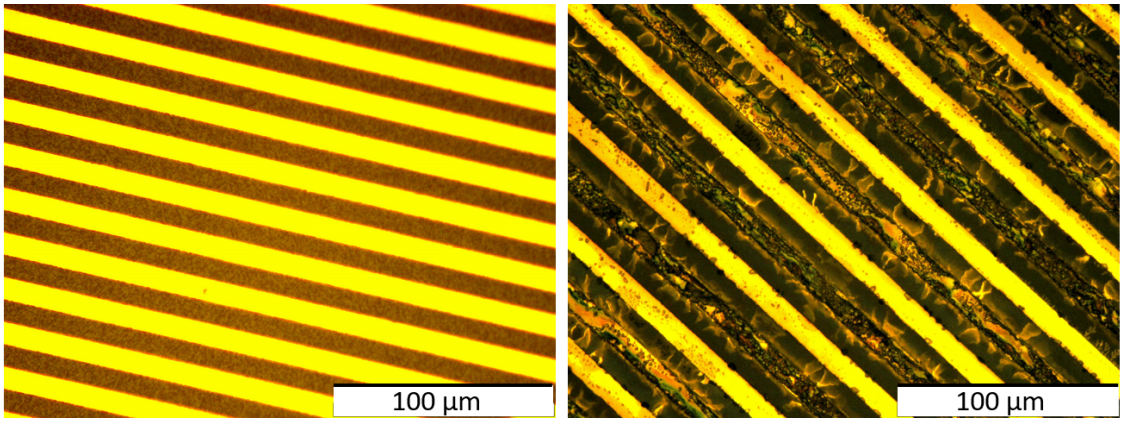

Figure 4.23: Both images are with a fiftyfold magnification from the same SVA experiment of Quinquethiophene on the Au-substrate. The left substrate has no voltage and the right substrate has a voltage of 20 V.

In fig. 4.24, the attachment to the positive ITO electrodes can be seen for quinquethiophene unlike for the molecules Ph-BTBT-10 and Ph-BTBTOx2, where no difference

was observed between the ITO substrates with and without voltage. In the left part of fig. 4.24 the fivefold magnification of the ITO substrate can be seen, where the inner two positive electrodes have a dark edge. The electrode with the dark edge is shown with a fiftyfold magnification in the right image. The dark substance is quinquethiophene which, as with the gold electrodes, attaches to the corners of the positive electrodes. Perhaps with these samples the experiment should be performed longer to see a larger effect, since the smallest distance between the ITO electrodes is five times larger than with the gold electrodes and thus the molecules diffuse longer to the positive electrode.

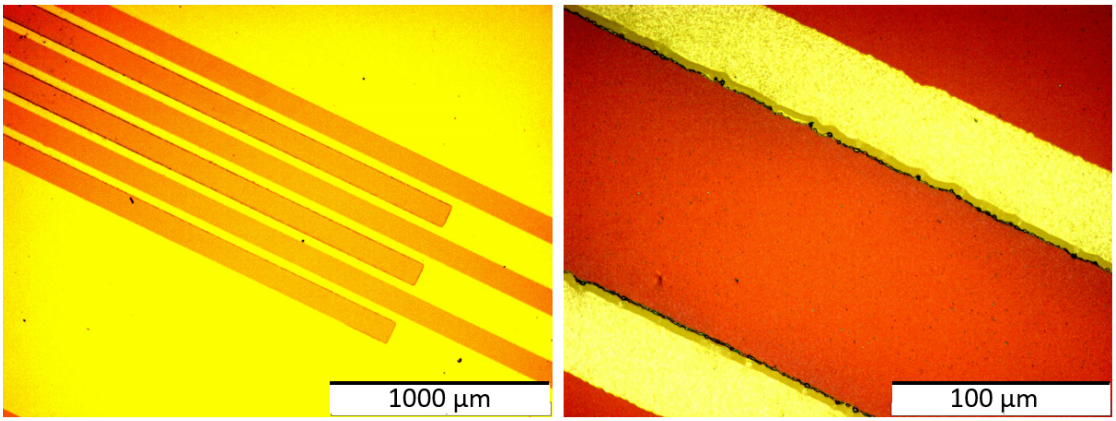

Figure 4.24: On the left is the optical microscope image with a fifefold magnification of quinquethiophene on the ITO substrate after SVA with 20 V. The right image shows the same sample with a fiftyfold magnification where the middle elctrode is the positive charged electrode.

4.3.2 Atomic force microscope

Fig. 4.25 shows the two gold substrates after PVD experiment with quinquethiophene with a film thickness of 27 nm, where on the left is the substrate without voltage and on the rigth is the substrate with a voltage of 150 V. For both substrates, as with the previous molecules, the collection is again at one corner of the electrodes. No other difference between the two substrates than the lower density of nucleation sites on the substrate with voltage is visible.

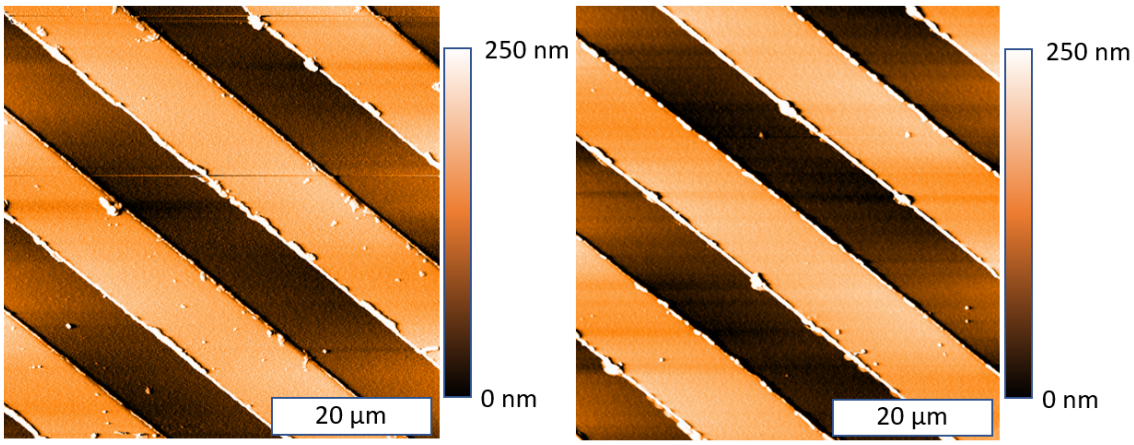

Figure 4.25: Both AFM images are from the same PVD experiment where on the left substrate no voltage is applied and it has about 45 nucleation sites and the right image is of the substrate with 150 V with about 20 nucleation sites.

Fig. 4.26 shows the substrates with a film thickness of 40 nm where the left image is the substrate treated without voltage and the right image is the substrate treated with a voltage of 30 V. On the left image again the the smooth surface with fewer nucleation sites is visible. Due to the larger film on the substrate compared to the other two molecules, the accumulation on the positive electrode (second from the rigth) is more visible on the substrate with voltage. The orientation between the electrodes is not measurable, but at the positive electrode a growth of the molecule along the gold layer can be seen. Instead of an orientation along an electric field we got after SVA an orientation along the gold electrodes, which implies that in terms of orientation, the substrate has a greater influence than the electric field.

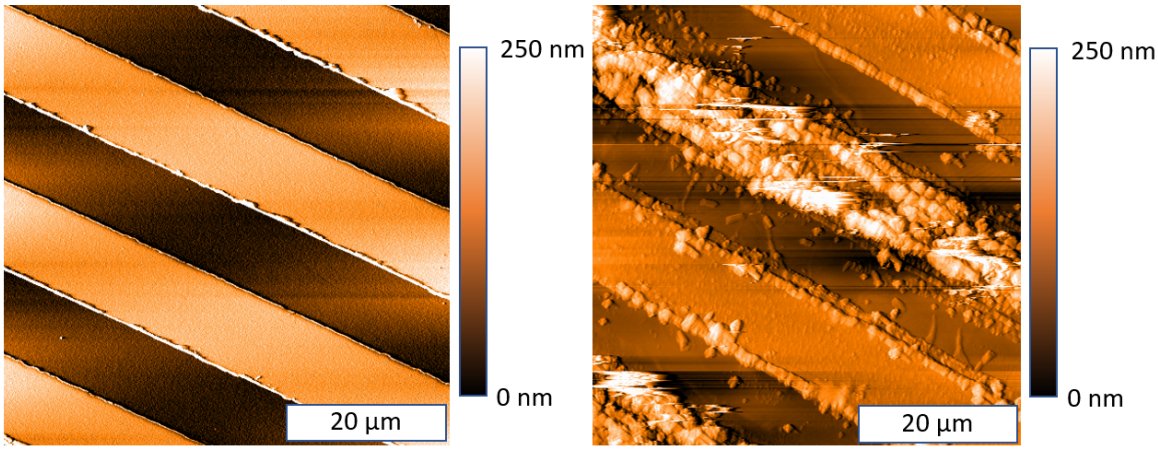

Figure 4.26: Both AFM images are from the same SVA experiment where the left substrate has no voltage and the right substrate has a voltage of 30 V.

4.3.3 X-ray reflectivity

As for the other molecules, the experimental setup for the molecule quinquethiophene also uses a 1/32 divergence slit, a 4 mm beam mask and a 0.1 mm anti-scatter slit but the measurement time is 48 min. Fig. 4.27 shows the diffraction spectrum of the molecule after PVD and after SVA, each with a substrate with and without voltage. No difference between the four variants is visible, thus neither the electric field nor the combination of electric field with chloroform have any influence on the out-of-plane orientation. The peak at $q = 0.300\mathring{A}$ is the 002 Bragg peak followed by an unknown peak. From the known crystal structure this peak could be only a lower order of the 021 peak, which is not possible. So probably there are two phases of quinquethiophene present.

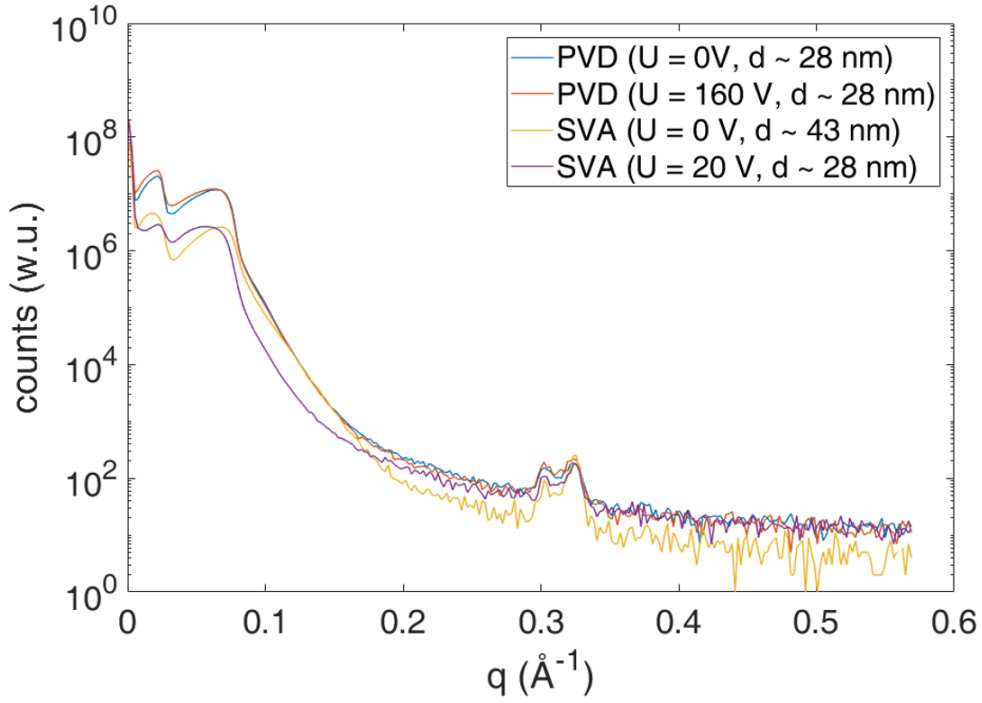

Figure 4.27: XRR spectrum of QQP after PVD at 0 V (blue) and 160 V (red) and after SVA at 20 V (orange)

4.3.4 Grazing incidence x-ray diffraction

As for the other two molecules for the GIXD measurement the incoming beam hit the substrate at an angle of 0.5° and the sample was rotated by 180° to measure the in-plane orientation as well. The measurement of the diffraction pattern is converted with the program GIDVis into the reciprocal space, where afterwards the peak positions and the peak intensities are analyzed. The ITO substrates were also measured but could not provide any information. Fig. 4.28 shows the reciprocal space map of quinquethiophene

on the Au-substrate after PVD with indexation with the known crystal structure assuming the 010 orientation. The bright peaks on the left edge are from the gold electrodes as well as the bright ring in the middle. The agreement of the intense peaks (112, 132, 133, 020 and 040) with the theoretical points are the evidence that the known crystal structure of quinquethiophene is on the substrate. There are also peaks, which do not agree with the known crystal structure, indicating that another phase is present.

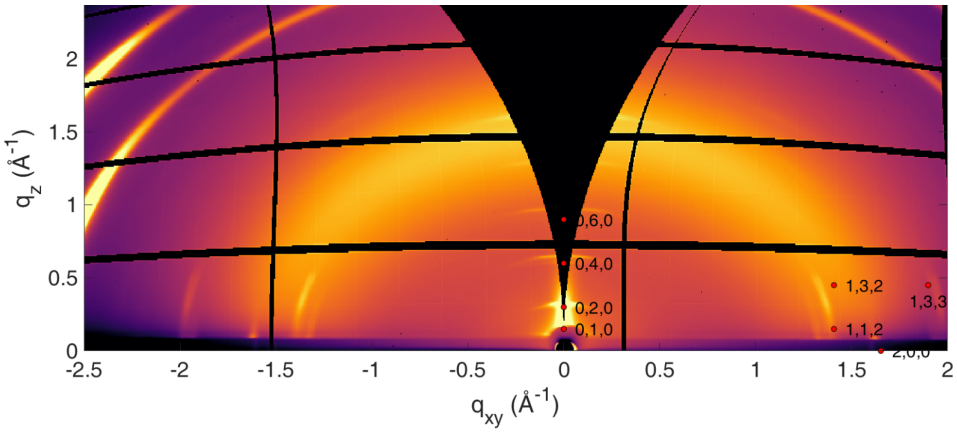

Figure 4.28: GIXD-Map of quinquethiophene on the gold substrate

As for Ph-BTBT-10 the in-plane orientation is analyzed, while the intensity of a strong peak at each rotation is summed up and plotted in a graph. The starting postion of the sample before rotating is that the gold electrodes are parallel to the incoming beam. Fig. 4.29 shows the dependence of the intensity of the 112 peak on the rotation of the substrate after the PVD experiment with a voltage of 160 V. The sample is rotated 180° in two degree increments. The intensity has nearly no changes after rotation and is nearly constant demonstrated with the black line, which means that there is only a weak in-plane orientation after PVD.

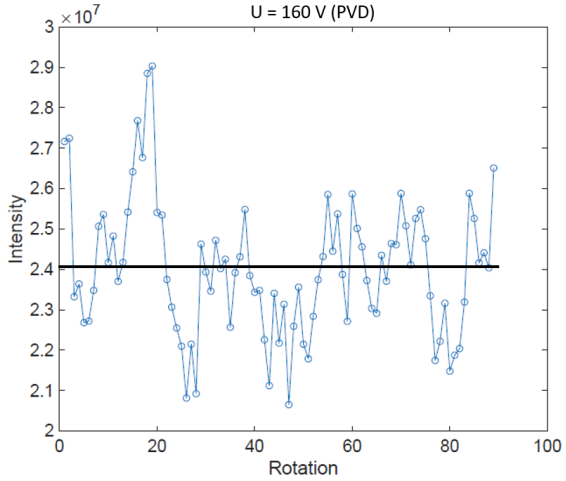

Figure 4.29: Intensity of the 112 peak from the 180 ° rotated Au-sample with quinquethiophene after PVD.

Fig. 4.30 shows the dependence of the intensity of the 112 peak on the rotation of the substrate but after the SVA experiment with a voltage of 20 V. The sample is rotated 180° in two degree increments, which means that by an rotation of 45 we have a rotation of 90°. The intensity drops after a rotation of 50° is reached and is lowest at 90° and starts to rise again after a rotation of 130° demonstrated with the two black lines. Since the intensity is lowest at 90°, the molecule is oriented in-plane in the direction of the gold electrodes and not in the direction of the electric field, because in this case the maximum intensity should be at 90° rotation.

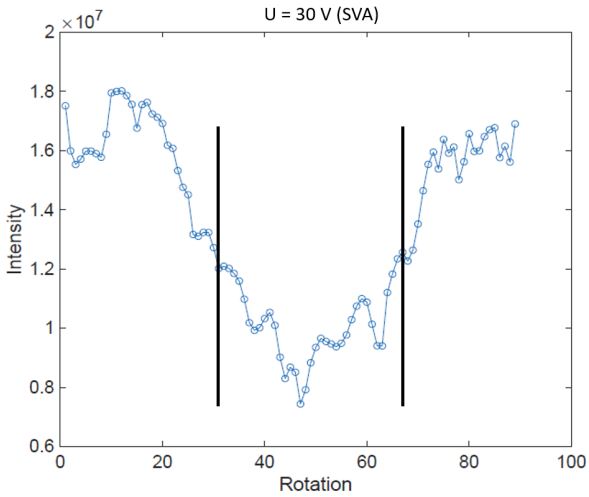

Figure 4.30: Intensity of the 112 peak from the 180 ° rotated Au-sample with quinquethiophene after SVA.

5 Conclusion

The aim of this work was to orient and control crystallization properties of three different organic semiconductor molecules on two different substrates with the help of an electric field. Two different methods of electric field orientation were used and the results were evaluated with an optical microscope, an atomic force microscope, X-ray reflection and grazing incidence X-ray diffraction. The molecules used are 2-decyl-7-phenyl-[1] benzothieno[3,2-b][1] benzothiophene (Ph-BTBT-10), 2-decyl-7-phenyl-[1]benzothieno[3,2-b][1]benzothiophene S,S,S',S'-tetraoxide (Ph-BTBTOx_2) and quinquethiophene. The methods for orientation with an electric field are physical vapor deposition and solvent vapor annealing on a glass substrate with gold electrodes or on a glass substrate with ITO electrodes.

In the PVD experiment, since the regulation of the deposition rate was hard to control and therefore two equal film thicknesses are difficult to be deposited. Furthermore, the SVA experiment always used substrates that had previously been coated by PVD, and therefore it was difficult to reproduce this experiment either, since the film thicknesses were always different.

All three molecules showed the same behavior after the PVD experiment, namely the number of nucleation sites is smaller in an environment surrounded by the electric field, which was confirmed with the optical microscope and with the AFM. Since the electric field has an effect not only on the number but also on the size of the crystals, in our experiment both effects could be demonstrated for Ph-BTBT-10 and Ph-BTBTOx_2. For the molecule Ph-BTBTOx_2, on the substrate with voltage, larger crystals collect at the corners of the electrodes than for the substrate without voltage. The molecule Ph-BTBT-10, on the other hand, showed only a few larger crystals in the AFM measurement, which prevents confirmation of the theory. In addition, the AFM was used to measure where the molecules condense. This was determined by a height difference measurement between glass and electrode. If the height difference after evaporation is larger than before evaporation, than the condensation occurs mainly on the electrodes. On the substrate without voltage, all three molecules condense equally over the entire substrate, unlike on the substrate with voltage. On this substrate these molecules condense more on the electrodes and less between them. Since there is no electric field on top of the electrodes to influence condensation, the electric field may reduce condensation between the electrodes. Furthermore, after the PVD experiment, neither optical nor XRR or GIXD measurements could detect the orientation of the molecules in a certain direction. The XRR pattern and also the space maps from the GIXD experiment look the same for the substrates with and without voltage.

After the solvent vapor annealing experiment, other effects occur. The first effect that occurs for all three molecules is an accumulation at the positive electrodes. The reason for this is that the molecules are probably deprotonated after the PVD experiment and thus become negatively charged. Furthermore, these molecules align in-plane along the electrode, which was confirmed with the intensity distribution of a peak of the rotating GIXD measurement. The molecules Ph-BTBT-10 and quinquethiophene do not grow along the electric field but only along the gold electrodes. For the molecule Ph-BTBTOx_2, on the other hand, a rod-like growth along the electric field is measured with the optical microscope. When evaluating the XRR data for quinquethiophene after the SVA experiment, there is no difference from the data after the PVD experiment. For the molecule Ph-BTBT-10, in contrast to the PVD measurement, the more stable bulk phase is observed after the SVA and for Ph-BTBT-Ox_2 a new phase appears after the SVA experiment, since the 001 Bragg peak is not at $q = 0.474\mathring{A}$ (known phase) but at $q = 0.415\mathring{A}$.

Comparing the two different substrates (Au and ITO), it can be seen that for the ITO substrate only one effect of the electric field on the crystallization was measured. Only in the case of quinquethiophene, when evaluated by optical microscope, after the SVA experiment, an accumulation of the molecules at the positive electrode can be seen, as is the case with the gold substrate. Also, the difference in height between the electrode and substrate could not be measured, since the width of the ITO electrode corresponds exactly to the maximum scanning range of the AFM. Other effects, such as the influence on the nucleation density or the orientation of the molecules after the PVD experiment are not present. On the one hand, this finding leads to the conclusion that, in the case of the gold substrate, perhaps the influence of the edge effects of the electrodes is greater than the influence of the electric field. If this is the reason, there should be no differences between the gold substrate with and without voltage, which is not the case. The reason that no differences can be measured between the substrate with and without voltage in the ITO substrate may be due to the larger distance between the electrodes.

List of Figures

Bibliography

[AR19] L. F. Alexander and N. Radacsi. “Application of electric fields for controlling crystallization”. In: *CrystEngComm* 21.34 (2019), pp. 5014–5031.

[BB13] W. H. Bragg and W. L. Bragg. “The reflection of X-rays by crystals”. In: *Proceedings of the Royal Society of London. Series A, Containing Papers of a Mathematical and Physical Character* 88.605 (1913), pp. 428–438.

[Bod+20] W. R. Bodlos et al. “Cold Crystallization of the Organic n-Type Small Molecule Semiconductor 2-Decyl-7-phenyl-[1] benzothieno [3, 2-b][1] benzothiophene S, S, S’, S’-Tetraoxide”. In: *Crystal growth & design* 21.1 (2020), pp. 325–332.

[DL+10] G. De Luca et al. “Solvent vapour annealing of organic thin films: controlling the self-assembly of functional systems across multiple length scales”. In: *Journal of Materials Chemistry* 20.13 (2010), pp. 2493–2498.

[Eba+07] H. Ebata et al. “Highly soluble [1] benzothieno [3, 2-b] benzothiophene (BTBT) derivatives for high-performance, solution-processed organic field-effect transistors”. In: *Journal of the American Chemical Society* 129.51 (2007), pp. 15732–15733.

[Ele] *XRD1 Beamline Description*. Website. Online https://www.elettra.trieste.it/lightsources/elettra/elettra-beamlines/xrd1/xrd1beamlinedescription.html; abgerufen am 27.04.2021. 2020.

[EW10] P. Eaton and P. West. *Atomic force microscopy*. Oxford university press, 2010.

[Far55] M. Faraday. “Experimental researches in electricity, vol. III”. In: *London, UK: Richard Taylor and William Francis* (1855), pp. 1846–1852.

[FKL13] W. Friedrich, P. Knipping, and M. Laue. “Interferenzerscheinungen bei roentgenstrahlen”. In: *Annalen der Physik* 346.10 (1913), pp. 971–988.

[Gwy] *Gwyddion*. Website. Online https://http://gwyddion.net/; Retrieved Jun 08,2021. 2020.

[Haj+97] R. Hajlaoui et al. “Improved field-effect mobility in short oligothiophenes: Quaterthiophene and quinquethiophene”. In: *Advanced Materials* 9.5 (1997), pp. 389–391.

[Hei16] J. Heintze. *Lehrbuch zur Experimentalphysik Band 3: Elektrizität und Magnetismus*. Springer-Verlag, 2016.

[Hof+21] S. Hofer et al. "Molecular Disorder in Crystalline Thin Films of an Asymmetric BTBT Derivative". In: *Chemistry of Materials* 33.4 (2021), pp. 1455–1461.

[Ibr+16] S. R. Ibrahim et al. "Naturally occurring thiophenes: isolation, purification, structural elucidation, and evaluation of bioactivities". In: *Phytochemistry reviews* 15.2 (2016), pp. 197–220.

[Ina08] K. Inaba. "X-ray thin-film measurement techniques". In: *The Rigaku Journal* 24.1 (2008), pp. 10–15.

[Inta] *Interdigitated electrodes (IDE)*. Website. Online https://www.micruxfluidic.com/en/electrochemical-solutions/thin-film-electrochemical-sensors/interdigitated-electrodes-ide/; abgerufen am 27.04.2021.

[Intb] *Interdigitated ITO Substrates for OFET and Sensing*. Website. Online https://www.ossila.com/products/interdigitated-ito-ofet-substrates?variant=1200244913; abgerufen am 27.04.2021.

[IUH15] H. Iino, T. Usui, and J.-i. Hanna. "Liquid crystals for organic thin-film transistors". In: *Nature communications* 6.1 (2015), pp. 1–8.

[Kas00] D. Kashchiev. *Nucleation*. Elsevier, 2000.

[Kie31] H. Kiessig. "Interferenz von Röntgenstrahlen an dünnen Schichten". In: *Annalen der Physik* 402.7 (1931), pp. 769–788.

[Kin] *Kinetic Theory*. Website. Online https://courses.lumenlearning.com/boundless-physics/chapter/kinetic-theory/; abgerufen am 27.04.2021.

[KOS16] K. Kotsuki, S. Obata, and K. Saiki. "Self-aligned growth of organic semiconductor single crystals by electric field". In: *Langmuir* 32.2 (2016), pp. 644–649.

[KTW19] C. Kommer, T. Tugendhat, and N. Wahl. *Tutorium Physik fürs Nebenfach*. Springer, 2019.

[KV65] C. H. Kruger and W. G. Vincenti. *Introduction to physical gas dynamics*. 1965.

[Ler+16] F Leroy et al. "How to control solid state dewetting: A short review". In: *Surface Science Reports* 71.2 (2016), pp. 391–409.

[Mah00] J. E. Mahan. *Physical vapor deposition of thin films*. 2000.

[Mit09] T. Mitsunaga. "X-ray thin-film measurement techniques". In: *Rigaku J* 25 (2009), pp. 7–12.

[MPL13] R. J. Martín-Palma and A. Lakhtakia. "Vapor-deposition techniques". In: *Engineered Biomimicry*. Elsevier Inc., 2013, pp. 383–398.

[MS77] J. Mullin and O Söhnel. "Expressions of supersaturation in crystallization studies". In: *Chemical Engineering Science* 32.7 (1977), pp. 683–686.

[PM13] E. M. Purcell and D. J. Morin. *Electricity and magnetism*. Cambridge University Press, 2013.

[Poh13] R. W. Pohl. *Elektrizitätslehre*. Springer-Verlag, 2013.

[Pol] *Molecular Shape and Polarity*. Website. Online https://chem.libretexts.org/@go/page/210718; Retrieved May 25,2021. 2020.

[Pvd] "Physical vapor deposition". In: *The Materials Science of Semiconductors*. Boston, MA: Springer US, 2008, pp. 505–572. ISBN: 978-0-387-68650-9. DOI: 10.1007/978-0-387-68650-9_11. URL: https://doi.org/10.1007/978-0-387-68650-9_11.

[Qqp] *alpha-Quinquethiophene*. Website. Online http://www.chemspider.com/Chemical-Structure.350594.html; abgerufen am 27.04.2021.

[Roc16] J. Roche. "Introducing electric fields". In: *Physics Education* 51.5 (2016), p. 055005.

[Rys02] P. V. Rysselberghe. "Remarks concerning the Clausius-Mossotti law". In: *The Journal of Physical Chemistry* 36.4 (2002), pp. 1152–1155.

[Sau59] G. Sauerbrey. "Verwendung von Schwingquarzen zur Wägung dünner Schichten und zur Mikrowägung". In: *Zeitschrift für physik* 155.2 (1959), pp. 206–222.

[SC93] D. Schwarzenbach and G. Chapuis. *Cristallographie*. Springer, 1993.

[Sch+15] G. Schweicher et al. "Bulky End-Capped [1] Benzothieno [3, 2-b] benzothiophenes: Reaching High-Mobility Organic Semiconductors by Fine Tuning of the Crystalline Solid-State Order". In: *Advanced materials* 27.19 (2015), pp. 3066–3072.

[SG13] F. Schreiber and A. Gerlach. "X-ray and neutron reflectivity for the investigation of thin films". In: *Website. www. physchem. ox. ac. uk/fs* (2013).

[SJ09] R. Serway and J. Jewett. *Physics for Scientists and Engineers*. Nelson Education, 2009.

[Tal+99] M Taleb et al. "Crystallization of proteins under an external electric field". In: *Journal of crystal growth* 200.3-4 (1999), pp. 575–582.

[The] *What is Thermal Annealing – Definition*. https://material-properties.org/what-is-thermal-annealing-definition. Eingesehen am 09.04.2021. URL: https://material-properties.org/what-is-thermal-annealing-definition.

[Tun] *Deep Cup Evaporation Boat*. https://www.lesker.com/newweb/evaporation_sources/thermal_boat_notched.cfm?pgid=4. Eingesehen am 07.04.2021. URL: https://www.lesker.com/newweb/evaporation_sources/thermal_boat_notched.cfm?pgid=4.

[Vás08] S. O. Vásquez. "A theoretical study of conformational aspects and energy transfer between terthiophene and quinquethiophene in perhydrotriphenylene inclusion compounds". In: *Physical Chemistry Chemical Physics* 10.35 (2008), pp. 5459–5468.

[Vel+17] G. Velpula et al. "Nanoscale control over the mixing behavior of surface-confined bicomponent supramolecular networks using an oriented external electric field". In: *ACS nano* 11.11 (2017), pp. 10903–10913.

[Wan+06] Y. Wang et al. "Real-time synchrotron x-ray studies of low-and high-temperature nitridation of c-plane sapphire". In: *Physical Review B* 74.23 (2006), p. 235304.

[WH95] C. Weißmantel and C. Hamann. *Grundlagen der Festkörperphysik*. Johann Ambrosius Barth Verlag, 1995.